Understanding the interaction between the co-chaperone DNAJC12 and tyrosine hydroxylase

Mary Dayne Sia Tai

This thesis is submitted in partial fulfilment of the requirements for the degree of Master of Science in Biomedical Sciences

Department of Biomedicine

Faculty of Medicine

University of Bergen

June 2020

Acknowledgements

If you had asked me three years ago where I would be and what I would be doing this 2020, I would never have guessed that I would be all the way across the world – in Norway, handing in this thesis in the midst of a worldwide pandemic. The past two years have been amazing and there are several people whom I would especially like to thank.

I would first like to express my utmost gratitude to Prof. Aurora Martinez, for giving me the opportunity to work on my thesis at the Biorecognition Laboratory, and without whom none of this would be possible. Thank you so much for your guidance and unending support. I have learned so much from you over the course of my Masters and for that, I am truly grateful.

I would also like to thank my thesis supervisors Marte Innselset Flydal and Kunwar Jung KC, who have gone over and beyond in supervising me for my thesis. Thank you so much for being so approachable and for not only teaching me the techniques in the laboratory, but also how to be a better scientist. I know that I get carried away sometimes but thank you for being so patient with me. I appreciate all your invaluable opinions, without which this thesis would not be how it is today.

I would also like to thank the whole of Lab E, especially Ming, Juha, Fredrik, Trond-André, Maite and Helene for sharing their inputs and expertise with me. I am very fortunate to have met and worked with every single one of you, Biorecognizers.

I am also very thankful to my co-graduate students here in Norway, especially Christer, Helene, Emma, Sayintha, Aishu, Leon and Ati, as well as those abroad and back home – Romie, Jessie, Zildjian, Elmo, and the ManICAlonggas who helped me keep my sanity when things were tough, for being great friends and for making my stay here so much better. I am also grateful for the Filipino friends I have made and for the family I accidentally found during the past two years – especially Tito Justo, Tita Alice, Eya and Jean. Thank you for all the laughter, the adventures and most especially for being my home away from home.

Lastly, I would like to thank my family back home in the Philippines, who despite the distance has always made me feel like I had never left. To my dad, mom, sister, brother and the rest of the family, thank you for all the love and support.

Table of Contents

List of Abbreviations

AAAH	aromatic amino acid hydroxylases
ATP	adenosine triphosphate
bp	base pair
CV	column volume
DLS	dynamic light scattering
EC	early eluting complex
EDTA	ethylenediaminetetraacetic acid
GST	glutathione S-transferase
HPA	hyperphenylalaninemia
HSP	heat shock protein
IMAC	immobilized metal affinity chromatography
IPTG	isopropyl β-D-1-thiogalactopyranoside
K_{av}	gel phase distribution coefficient
K_D	equilibrium dissociation constant
kDa	kilodaltons
k_{off}	dissociation rate constant
k_{on}	association rate constant
LB	Luria-Bertani broth
LC	late eluting complex
MBP	maltose binding protein
MS/MS	tandem mass spectrometry
MWCO	molecular weight cut-off
PAH	phenylalanine hydroxylase
PCR	polymerase chain reaction
SD	standard deviation
SDS-PAGE	sodium dodecyl sulfate polyacrylamide gel electrophoresis
SE	standard error
SEC	size exclusion chromatography
SEC-MALS	size exclusion chromatography coupled with multi-angle light scattering
SPR	surface plasmon resonance
TB	terrific broth
TEV	tobacco etch virus
TH	tyrosine hydroxylase
THD	tyrosine hydroxylase deficiency
TPH	tryptophan hydroxylase
V_e	elution volume
V_o	void volume
V_t	total bed volume

Summary

Tyrosine hydroxylase (TH) catalyzes the rate-limiting step in the biosynthesis of the catecholamines dopamine, adrenaline and noradrenaline. Dysfunctional TH due primarily to mutations in the *TH* gene may lead to motor and neurological disorders observed in tyrosine hydroxylase deficiency (THD) patients. Some disease variants of TH have been found to result in enzymes with decreased stability or activity, and others with altered substrate specificity.

DNAJC12 is an HSP40 co-chaperone protein which works with molecular chaperones of the HSP70 family to maintain protein homeostasis by promoting refolding and degradation of client proteins. TH and the other aromatic amino acid hydroxylases were recently identified as clients of DNAJC12. Not much is known on the structure of this protein, apart from the highly conserved N-terminal J-domain that is common to all DNAJ proteins and crucial for proper HSP70-client interaction.

In this work, human DNAJC12 was expressed in bacteria and purified with the aim of characterizing its interaction with TH on a molecular level. This is, to our knowledge, the first time DNAJC12 has been studied *in vitro*. Size exclusion chromatography (SEC) and dynamic light scattering (DLS) analyses showed that DNAJC12 is composed mainly of what appears to be a dimer under the experimental conditions, but also larger oligomers.

Binding studies using analytical SEC, SEC coupled with multi angle light scattering (SEC-MALS), surface plasmon resonance (SPR) and DLS demonstrated that DNAJC12 forms a complex with the human tyrosine hydroxylase isoform 1 (hTH1) at both low and physiological temperatures, and that this interaction can delay hTH1 aggregation *in vitro*. Only full-length DNAJC12 and a C-terminal fragment of this protein were identified in the complex, supporting the hypothesis that the C-terminal region is responsible for client binding. The apparent dimeric form of DNAJC12 bound to hTH1 with high affinity, as the estimated equilibrium dissociation constant was in the 10^{-1} μM range. Further characterization of the DNAJC12-hTH1 complex can increase our understanding on the regulation of hTH1 intracellular stability and may provide novel targets for the treatment of underlying neurometabolic disorders.

1 Introduction

Proteins are macromolecules found in all living organisms that are required in a myriad of biological reactions necessary for proper cell function, structure, and regulation. Approximately 20,000 to 25,000 different proteins are involved in biological function in humans and the coordinated interactions of these proteins are vital for the correct execution of their specific functions (reviewed in [1, 2]). These protein-protein interactions are facilitated by hydrogen bonding, van der Waals forces, as well as electrostatic and hydrophobic interactions that result in specific or non-specific intermolecular interactions that can be transient or sustained [3]. In order to achieve proper functionality, proteins must fold into specific three-dimensional structures, also known as their native states, either spontaneously or with the assistance of molecular chaperones [2, 4]. Failure to fold into the native state can result in non-native interactions such as aggregation that may hinder proper protein function [2, 4, 5]. Maintaining protein homeostasis is therefore essential in preserving proteome fidelity that is crucial for cellular function and the overall preservation of organismal health [6, 7].

1.1 Protein Homeostasis

Protein homeostasis or proteostasis refers to the upkeep of correct protein macromolecular concentration, conformation and subcellular localization that leads to a dynamic equilibrium where protein synthesis and folding are balanced with degradation [6]. Therefore, in order to maintain protein homeostasis in the cell, tight regulation of protein biogenesis, folding, trafficking and degradation is required, which involves the coordinated interaction of more than 2,000 proteins in human cells [8]. Studying the mechanisms behind the organization and regulation of this extensive proteostasis network – such as molecular chaperones and co-chaperones of the quality control machinery – may reveal key information that can aid in the understanding of diseases associated with the loss of proteostasis.

1.1.1 Protein Folding

Proteins encoded on messenger RNAs are synthesized by ribosomes as linear chains of amino acids, which then fold into energetically favorable well-defined three dimensional structures that are necessary for their proper function [2, 4]. Not all proteins are able to properly

fold into their native states spontaneously and may therefore require molecular chaperones that assist by preventing non-native interactions and by keeping client proteins accessible to re-folding or degradation [9]. Ribosome-associated chaperones also bind to nascent polypeptide chains and facilitate folding, translocation or interaction with other chaperones as well as prevent undesirable inter- or intra-chain contacts that can result in misfolding and aggregation [10].

Studies on ribonuclease by Christian Anfinsen in the 1970s demonstrated that proteins can spontaneously re-fold *in vitro* after denaturation, suggesting that the native conformation of proteins was intrinsic and solely influenced by the amino acid sequence [11]. Mutations in the primary sequence therefore make it more likely for the protein to misfold and engage in non-native interactions. More recent studies, however, have demonstrated that proteins can misfold or form aggregates even without having mutations in the primary sequence, an event that increases in aging, suggesting that the native state of a protein is not only dependent on its amino acid sequence but can be influenced by the highly dynamic network of interactions that governs proteostasis [7].

A balance between thermodynamic stability and conformational flexibility is necessary to define the native conformation of a protein [4]. Each amino acid chain may adopt a large number of possible conformations and thus folding reactions are regulated by multiple non-covalent interactions such as hydrophobic forces that propel non-polar amino acid residues to bury into the protein interior [2, 9].

Larger proteins that contain more than 100 amino acids have the tendency to fold into non-native folding intermediates, which may either be "on-pathway" conformations toward the native state or stable, misfolded conformations that may require extensive reorganization to reach the native state [12]. Reorganization of these intermediates is hindered by kinetic barriers which molecular chaperones can help overcome [12]. Chaperones also aid in preventing intermolecular interactions such as the formation of amorphous aggregates, oligomers and fibrils [2] (Figure 1-1).

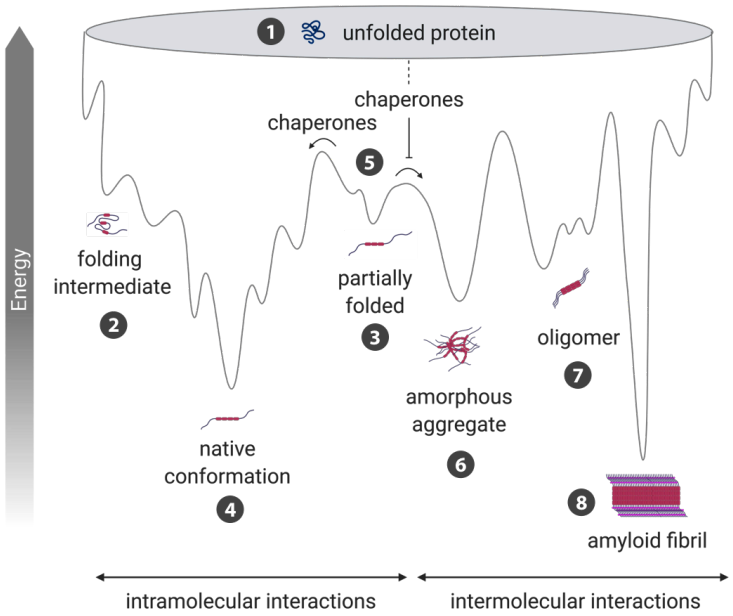

Figure 1-1 Energy landscape schematic of protein folding and aggregation. Newly synthesized proteins are unfolded (1) and can either fold spontaneously via folding intermediates (2) or adopt partially folded non-native structures (3) which must be reorganized into the native structure (4). During reorganization, these structures must overcome kinetic barriers *en route* to their native states. Chaperone proteins raise the free energy, helping the intermediates to overcome these kinetic barriers (5) [13]. Chaperones also prevent the formation of aggregates (6), oligomers (7) and fibrils (8) through steric hindrance. This interaction promotes folding into the native state by keeping clients accessible for other chaperones and machinery involved in re-folding or degradation. Without chaperones, these large molecules are more likely to be formed and can result in toxic aggregation and eventually disease. The formation of fibrils, for example, is a hallmark of several neurological diseases such as Parkinson's and Alzheimer's [6, 14]. Modified from [12] and illustrated using BioRender.

1.1.2 Degradation

Along with regulated protein synthesis and folding, controlled degradation is a key mechanism that regulates cellular processes and promotes protein homeostasis. Terminally misfolded proteins and aggregates are usually degraded rapidly to avoid toxic accumulation, while functional proteins are degraded to regulate cellular processes and to facilitate protein turnover. Proteins undergo degradation through two major pathways: the ubiquitin-proteasome system (UPS) and the autophagosomal-lysosomal pathway [15]. The UPS is an ATP-dependent system that targets single molecules by tagging them with either a single ubiquitin subunit (monoubiquitination) or a chain of ubiquitin subunits (polyubiquitination). Ubiquitinated proteins are then recognized by the proteasome, which degrades the proteins into small peptides [13, 15]. Rather than degrading single targets, the autophagy-lysosomal system is capable of degrading larger molecules such as aggregates and organelles [16]. Targets are enclosed in vesicles which fuse with lysosomes containing proteolytic enzymes. Both systems, however, may require molecular chaperone proteins that recognize and keep targets accessible to degradation [5].

1.1.3 Molecular Chaperones

Molecular chaperones are ubiquitous proteins that are involved in maintaining protein homeostasis and controlling protein quality in the cell [17]. Classifications of chaperones, also called heat shock proteins (HSPs) are largely based on sequence homology and molecular weight, with the major classifications being the HSP40, HSP60, HSP70, HSP90, HSP100 and the small HSP (sHSP), where the number represents the molecular weight of the complete protein [2]. These HSPs may act alone or in concert with co-chaperones to not only maintain protein homeostasis by folding nascent polypeptides, but also to control protein quality by assisting in refolding, facilitating disaggregation and targeting degradation of proteins [1, 2, 17]. The most abundant chaperone proteins are the HSP70s and HSP90s, which are estimated to comprise approximately 1-2% of the total proteome of some cells [5]. Client specificity and activity of these chaperones are heavily influenced by their interactions with co-chaperones. Over 20 co-chaperones have been found to associate with HSP90s, while HSP70s mostly interact with HSP40s, which are considered as co-chaperones [18].

1.1.4 HSP40 Family (DNAJ Proteins)

HSP40s, also known as the DNAJ family of co-chaperone proteins or J-proteins, are HSPs that function by recognizing and binding specific clients and presenting them to HSP70s for re-folding or degradation [19] (Figure 1-2). All HSP40s have a conserved J-domain consisting of approximately 70 amino acids that fold into four α-helices [20] (Figure 1-3A). The tripeptide histidine, proline, and aspartic acid (HPD motif) is a highly conserved sequence located in the loop between the second and third helices. The HPD motif, along with client binding, is necessary for stimulating ATPase activity in HSP70s, which is essential to stabilizing the substrate-HSP70 interaction [20, 21].

Apart from the J-domain, there is little similarity among the approximately 50 members of the DNAJ family and their diversity greatly expands the range and specificity of HSP70 function. This explains the implication of HSP70 in diverse cellular functions, despite only 13 different types of the protein being encoded in the human genome [22]. The HSP40s in humans ranges in size from 12.5 kDa (DNAJC19) to 505 kDa (DNAJC29) as they have evolved to contain different domains necessary to increase variation for client targeting and general function [14, 22].

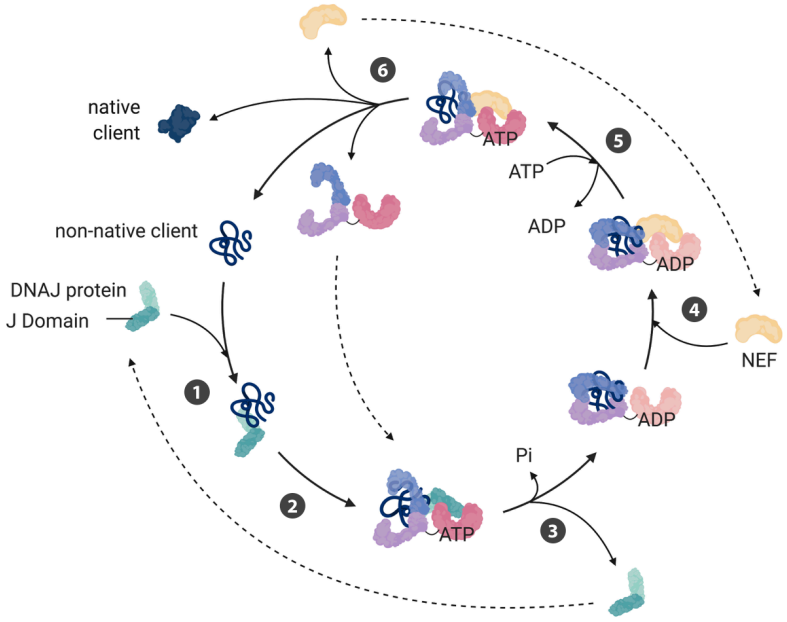

Figure 1-2. The canonical HSP70/DNAJC12 chaperone system. The DNAJ protein recognizes and binds to its client, inducing a conformational change that makes the client more accessible to HSP70 binding [23, 24] (1). DNAJ-client complex binds to HSP70-ATP via the J-domain of the DNAJ-protein (2). DNAJ HPD motif interacts with key residues in the HSP70, stimulating HSP70 ATPase activity which results in the hydrolysis of ATP to ADP in the nucleotide binding cleft and the subsequent dissociation of the DNAJ protein [25]. This results in a conformational change in HSP70 which locks the substrate into the substrate binding cleft of the HSP70 (3). The nucleotide exchange factor (NEF) then binds to HSP70-ADP, causing conformational changes in the HSP70 (4), leading to the the removal of ADP and subsequent binding of ATP which results in conformational changes that open the substrate binding cleft of the HSP70 (5). The HSP70-ATP and NEF complex dissociates and can be re-used to either fold other clients or re-fold the same substrate if necessary (6). Figure modified from [19] and illustrated using BioRender.

J-proteins are further categorized based on their additional domains resulting in three main categories: class I, class II and class III (or A, B and C, respectively) [24] (Figure 1-3B). DNAJA or class I J-proteins are those with an N-terminal J-domain followed by a flexible Glycine/Phenylalanine (G/F) rich linker region, four repeats of the CxxCxGxG type zinc finger, and an extended C-terminal region, necessary for dimerization and client binding [19, 20, 24]. DNAJB or Class II J-proteins also have the N-terminal J-domain followed by the G/F rich region, but not the zinc finger motif. Other proteins that have the J-domain but cannot be categorized under the two described types are then classified as DNAJC or Class III J-proteins [19, 20].

Among the three classes of J-proteins, the DNAJC subfamily is the largest and most diverse, consisting of 32 members [14, 22]. DNAJCs have protein sequences ranging from 116-4432 amino acids in length and have been implicated in a variety of functions as well as in disease [22]. For example, dysfunctional DNAJC6 has been identified in patients with early onset Parkinson's disease. DNAJC6 is involved in clathrin uncoating, which when

dysregulated results in decreased synaptic vesicle recycling and endocytosis [26, 27]. Mutations in DNAJC21, on the other hand, lead to the accumulation of its client resulting in abnormal ribosome profiles and cell death, which contribute to bone marrow failure syndrome [28].

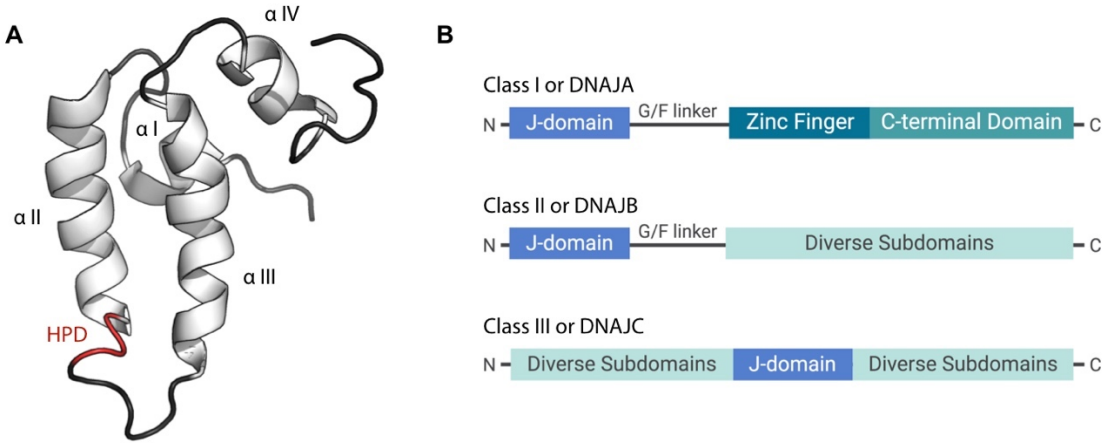

Figure 1-3. DNAJ Proteins. (A) Structure of the J-Domain. (PDB ID 1BQ0). The HPD domain is highlighted in red and the four helices are labelled from α I-IV. (B) Organization of Class I, II and III DNAJ proteins. Modified from [24]. Illustrated using Pymol.

1.2 Misfolding Diseases

Many proteins fail to achieve their native states due to mutations in their sequences, failure in targeted re-folding or degradation, as well as when exposed to heat, oxidative stress or toxic substances [18, 29]. Misfolded proteins can cause diseases through either a loss- or gain-of-function mechanism of pathogenesis. Loss-of-function pathogenesis is associated with increased rates of degradation, whereas gain-of-function pathogenesis is associated with the accumulation and formation of toxic aggregates [30]. For example, the misfolding disease cystic fibrosis is considered to be caused by loss-of-function mutations in the cystic fibrosis transmembrane regulator (CFTR) protein, as the protein products are immediately targeted for degradation, despite having residual activity, and toxic aggregates are not accumulated [31].

In misfolding diseases with a gain-of-function pathogenesis, the increased susceptibility of misfolded proteins to aggregate along with the failure of the proteostasis network to clear these proteins either by re-folding or degradation result in their toxic accumulation [13, 17]. Protein aggregation inside the cell can lead to formation of amyloid-like structures (Figure 1-1), which can cause various degenerative disorders and cell death [29]. For example, patients

with Alzheimer's disease have been observed to have protein aggregates in the cerebral cortex, which is currently considered as one of the hallmarks of neurodegenerative diseases [32]. The aggregation of proteins, however, is not confined to the nervous system, and can also cause non-neurodegenerative disorders such as type II diabetes [33]. The implication of proteostasis deficiency in disease and recently, in aging, highlights the increasing importance of understanding proteostasis network(s) [6, 7].

1.2.1 Phenylketonuria – A Misfolding Metabolic Disease

PAH converts L-phenylalanine (L-Phe) to L-tyrosine (L-Tyr) using tetrahydrobiopterin (BH_4) as cofactor, and its dysfunction causes neurotoxic accumulation of L-Phe [34]. Most of the >1000 described PKU mutations result in misfolding and destabilization of the protein, which leads to the loss of enzymatic function [35].

However, hyperphenylalaninemia (HPA; accumulation of L-Phe), may not only be caused by deficient PAH activity, but also by abnormalities in the processes and enzymes related to BH_4 synthesis and recycling [36, 37]. Recently, mutations in the co-chaperone DNAJC12 were also found to result in phenotypic manifestations of HPA, suggesting that PAH dysfunction could not only be caused by mutations in *PAH* or in BH_4-associated genes, but can also be influenced by mutations in proteins related to the proteostasis network. All four aromatic amino acid hydroxylases (AAAHs) were recently identified as clients of the co-chaperone [38, 39]. A similar mechanism could be present in tyrosine hydroxylase deficiency (THD), a disease caused by mutations in the AAAH tyrosine hydroxylase (TH) [40].

1.3 Aromatic Amino Acid Hydroxylases (AAAHs)

The aromatic amino acid hydroxylases (AAAHs) are a family of iron(II) dependent enzymes consisting of four members that share similar catalytic, structural and functional characteristics [41]. These four enzymes are PAH (see 1.2.1), TH and tryptophan hydroxylases 1 and 2 (TPH1 and TPH2). Along with the cofactor BH_4 and the additional substrate molecular oxygen, these AAAHs catalyze the hydroxylation of aromatic amino acids. PAH converts L-Phe to L-Tyr, which is then converted by TH to L-dihydorxyphenylalanine (L-DOPA). The TPHs, on the other hand, convert tryptophan to 5-hydroxytryptophan, which is a precursor of serotonin and melatonin [42]. Mutations in these enzymes have been implicated in diseases, suggesting their crucial roles in proper neurological and metabolic function. As mentioned

before, mutations in PAH cause PKU, while those in TPH have been linked to several diseases such as schizophrenia and Tourette's syndrome [43, 44] and mutations in TH lead to tyrosine hydroxylase deficiency (THD) (Section 1.4.3) [45].

1.4 Tyrosine Hydroxylase

TH hydroxylates L-Tyr to L-DOPA, which is the rate-limiting reaction in the biosynthesis of catecholamines dopamine, noradrenaline and adrenaline [46]. These catecholamines function as both hormones and neurotransmitters, which are crucial for normal nervous system function. Four main isoforms of TH have been identified in humans, which are formed by TH pre-mRNA alternative splicing [47]. TH isoforms 1 and 2 (hTH1; hTH2) are the most abundant forms and are highly expressed in the brain and adrenal medulla [48].

1.4.1 Structure of Tyrosine Hydroxylase

In solution, TH forms a ~240 kDa homotetramer, where each ~60 kDa subunit consists of a regulatory ACT domain with an N-terminal tail, a catalytic domain, and a C-terminal oligomerization domain [49]. The TH tetramer assembles via the C-terminal oligomerization domain that forms a hydrophobic core. The catalytic domain includes the active sites for iron, cofactor and substrate binding. [48]. The full length structure of the tetramer has recently been elucidated by small-angle x-ray scattering (SAXS) [49] (Figure 1-4).

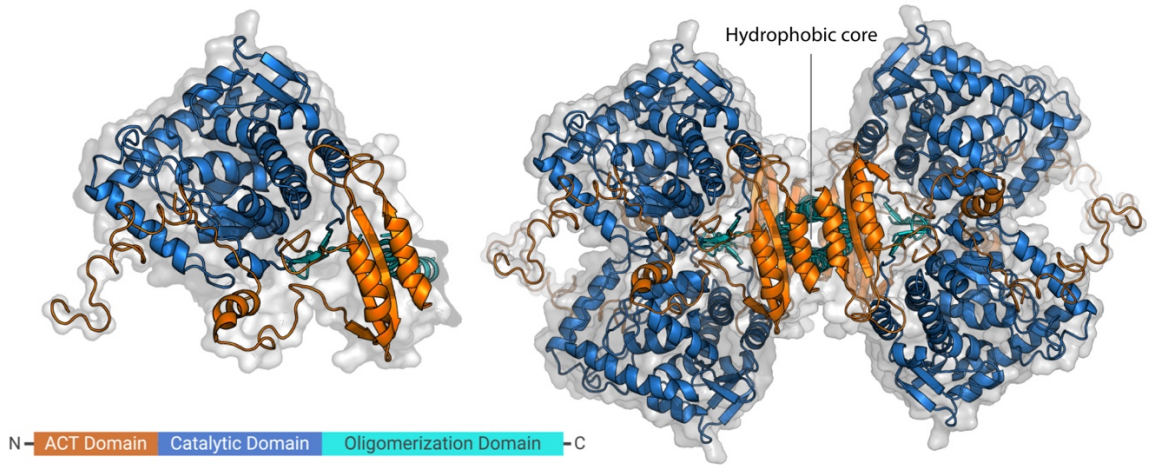

Figure 1-4 The structure of full-length TH elucidated by SAXS. TH is a homotetrameric protein. Each subunit contains an N-terminal regulatory ACT domain, a catalytic domain and a C-terminal oligomerization domain forming a tetramerization helix-bundle. (SASBD ID: SASDBZ4) Modified from [49].

1.4.2 Regulation of Tyrosine Hydroxylase

Catecholamine synthesis is a highly regulated process that can be controlled by feedback and post-translational regulatory mechanisms. TH enzymatic activity is feedback inhibited by the binding of catecholamines to its active site and is post-translationally regulated by phosphorylation by various kinases at residues Ser/Thr 8, Ser19, Ser31 and Ser40, which are all located at the N-terminal region [48, 50]. Phosphorylation at Ser40 and Ser31 are reported to increase TH activity, while no effect has been reported for Ser/Thr8 [51-53]. The mechanism by which Ser40 phosphorylation increases TH activity is the most understood, and involves the reversal of catecholamine binding and increased affinity for BH_4 [51, 54]. Weak TH activation was also observed by Ser19 phosphorylation alone, but is increased with the binding of the regulatory protein 14-3-3 [55]. Phosphorylation of Ser31 has also recently been reported to influence TH subcellular localization to the axon terminal, indicating that phosphorylation can regulate TH by a mechanism other than affecting its enzymatic activity [56].

1.4.3 Tyrosine Hydroxylase Deficiency

Mutations in *TH* are associated with THD, which is an autosomal recessive disorder that mainly presents as DOPA-responsive dystonia or infantile parkinsonism with a varying clinical spectrum [50]. There are more than 40 identified disease-related mutations and most mutants show decreased solubility or activity, while others exhibit altered substrate binding [45]. Recent studies on *Th*-knock-in mice with the mutation R203H (human TH-R233H; hTH1-R202H) suggest that mutant TH is misfolded and unstable, resulting in dysfunctional enzymes that lead to altered levels of catecholamines [40]. These, in turn, result in abnormal nervous system function that causes autonomic dysfunction, abnormal movements and other neurological problems that can range from mild to severe, which are often observed in THD patients [48].

1.5 DNAJC12

DNAJC12, also known as J-domain containing protein 1 (JDP1), is a co-chaperone protein recently identified as a potential binding partner of the AAAHs [38, 39, 57]. DNAJC12 is a 24 kDa HSP40 Class III protein comprised of 198 amino acids that is mostly localized in the cytoplasm [57, 58]. Only the structure of the first 100 amino acids, which contains the

highly conserved J-domain, has so far been elucidated by NMR (PDB ID 2CTQ; Figure 1-5). Apart from its J-domain, no other conserved domains are predicted in its sequence.

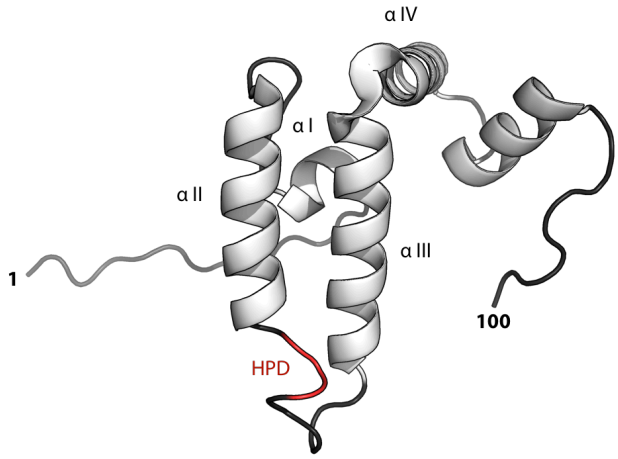

Figure 1-5. The partial structure of DNAJC12, containing the J-domain (PDB ID 2CTQ). Structure of the first 100 amino acids of DNAJC12 resolved by NMR. The 4 helices of the J-domain are numbered I-IV. The HPD motif is highlighted in red. Illustrated using Pymol.

The *DNAJC12* gene is 1,221 base pairs long, has 5 exons and is located at the chromosome region 10q21.3 [59]. The gene is expressed in several tissue types but has been found to have the highest levels of expression in the brain, adrenal gland, pituitary and liver [60, 61]. DNAJC12 was also observed to be upregulated in cells during ER stress and as an HSP40 protein, is believed to cooperate with HSP70 for client targeting, re-folding and degradation [38, 58, 62].

Variants of DNAJC12 were recently identified in patients presenting with HPA without having mutations in the *PAH* or BH4-associated genes [38]. Since then, more and more cases of individuals with varying clinical spectra suffering from HPA, dystonia or intellectual disabilities with mutations in DNAJC12 have been identified [63-68].

DNAJC12 has been further implicated in other diseases, suggesting its important role beyond the AAAHs. DNAJC12 was found to be upregulated in triple negative breast cancer tumors and has been correlated with poor prognosis in patients [69]. Overexpression of DNAJC12 was also implicated in tumor progression and aggressive phenotypes in colorectal cancer, as well as in poor responses to neoadjuvant concurrent chemoradiotherapy [70]. Furthermore, DNAJC12 was also found to be upregulated in aggressive forms of gastric cancer. Analysis of the transcriptome correlated high DNAJC12 expression with lymphatic invasion,

metastasis and general gastric cancer progression leading to higher mortality rates in patients [71]. siRNA-mediated *DNAJC12* silencing also revealed reduced proliferation and invasion of gastric cancer cells, further implicating DNAJC12 in cancer progression [71]. However, the exact mechanisms of DNAJC12 function in these cancer forms are still unknown.

2 Aims

Mutations in the co-chaperone DNAJC12 have recently been found in patients with hyperphenylalaninemia, dystonia and movement disorders. The aromatic amino acid hydroxylases have been identified as the specific clients of this co-chaperone which, as an HSP40, is likely to cooperate with HSP70s and target clients for re-folding and degradation. Not much is known about DNAJC12, and this is, to our knowledge the first time it has been studied *in vitro*. Therefore, the primary objective of this study was to gain insights into the structure and function of the co-chaperone DNAJC12, as well as the structural determinants and effects of the interaction with its client, tyrosine hydroxylase (TH). We intended to do this by the following sub-aims:

1. To develop the bacterial expression and purification of recombinant DNAJC12.
2. To determine the oligomeric organization of recombinant DNAJC12.
3. To validate the interaction of DNAJC12 and TH *in vitro* and prepare samples to determine the structure of the complex.
4. To gain insights into the mechanism of the interaction between DNAJC12 and TH.
5. To obtain preliminary data on the function of DNAJC12, especially its role in the proteostasis of client proteins.

3 Methodological Considerations

3.1 Plasmids

The pETGST1a, pETMBP1a and pETZZ1a empty vectors were obtained from pETGST1a/*YFP*, pETMBP1a/*hTH1* and pETZZ1A/*hTH1* by simultaneous double digestion using NcoI and Acc65I restriction enzymes (Figure 3-1). The pETMBP1a/*hTH1* and pETZZ1A/*hTH1* plasmids were previously derived from the original pETMBP1a/*YFP* and pETZZ1a/*YFP* plasmids [49], and the pETMBP1a/*hTH1* was used for recombinant human tyrosine hydroxylase isoform 1 (hTH1) expression. The pETGST1a/*YFP*, pETMBP1a/*YFP* and pETZZ1a/*YFP* plasmids were gifts from Gunter Stier (EMBL, Heidelberg, Germany) [72]. All three vectors have the kanamycin resistance (*KanR*) gene to enable antibiotic selection, the *lac* operon that controls fusion protein expression which can be induced by the addition of isopropyl β-D-1-thiogalactopyranoside (IPTG), and the tobacco etch virus (TEV) protease cleavage site ENLYFQ(G/S), which is encoded between the tags and the cloned gene.

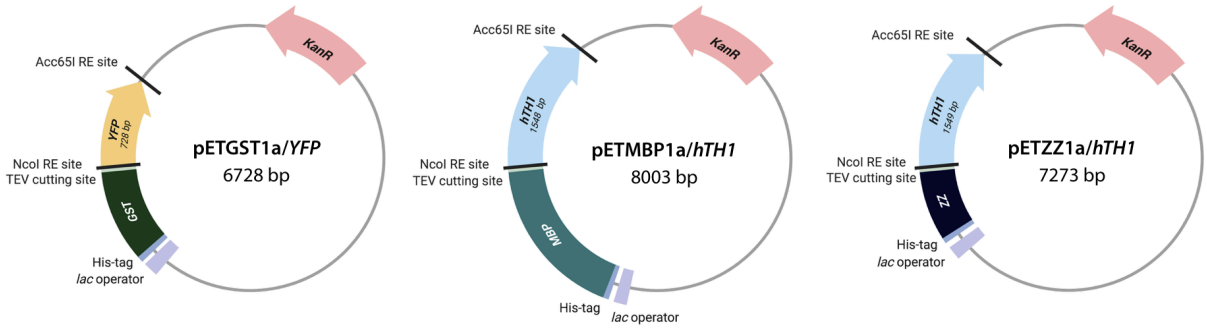

Figure 3-1 Simplified pETGST1a/*YFP*, pETMBP1a/*hTH1* and pETZZ1a/*hTH1* plasmid maps. *YFP* or *hTH1* cDNA were cloned at the C-terminus of HisGST, HisMBP or HisZZ prior to this work. The open reading frames for the fusion proteins and kanamycin resistance (*KanR*) are shown as arrows. The NcoI and Acc65I restriction enzyme cutting sites, *lac* operon and TEV protease cleavage sites are also indicated in the figure.

3.2 Sodium dodecyl sulfate Polyacrylamide Gel Electrophoresis

SDS-PAGE is an electrophoretic technique which separates denatured proteins by molecular weight. Samples are denatured by the addition of sodium dodecyl sulfate (SDS), which is an amphipathic surfactant that linearizes proteins by binding to and exposing hydrophobic regions that would normally be buried into the protein interior. SDS binding also results in a uniform negative charge by binding to proteins in proportion to their respective

molecular weights [73]. Aside from the addition of SDS, the proteins are also further denatured by the addition of the reducing agent dithiothreitol (DTT) and by heating at 95 °C, which disrupt disulfide linkages as well as intra- and inter- molecular interactions. These denaturing steps allow the migration of proteins through the polyacrylamide matrix towards the positive electrode at a rate that is almost only influenced by their respective molar masses [73].

3.3 Western Blot

Western blot or protein immunoblotting is an analytical technique that utilizes the highly specific antigen recognition properties of antibodies to detect the presence of the target protein in a sample. Upon denaturation, protein samples are separated by SDS-PAGE based on their molecular size and are transferred on to either polyvinylidene difluoride (PVDF) or nitrocellulose membrane (PVDF was used in this work) which is subsequently blocked by 5% whole milk to prevent non-specific binding. The samples in this work were analyzed by an indirect method of detection, which makes use of a primary antibody that recognizes an epitope on a target protein, and a secondary antibody that binds to the primary antibody. In this work, the secondary antibodies used were conjugated to horseradish peroxidase (HRP), which in the presence of strong oxidizing agent such as hydrogen peroxide, can oxidize the substrate luminol thus emitting light as a byproduct of the reaction.

3.4 Affinity Chromatography

Affinity chromatography is a biophysical technique used to efficiently separate or purify components in a given mixture based on their specific interactions with an immobilized substrate (Figure 3-2) [74]. In this study, two types of affinity chromatography are used for protein purification: amylose affinity chromatography using amylose resin and immobilized metal ion affinity chromatography (IMAC) using TALON® resin.

Amylose affinity chromatography is a technique used to purify maltose binding protein (MBP)-tagged recombinant proteins [74]. MBP interacts with the α-(1→4)-maltodextrins in the amylose resin and can be eluted by addition of maltose [75]. As MBP has a higher binding affinity for maltose than for amylose, the fusion protein is released from the amylose resin [75]. IMAC using TALON® resin is used to purify proteins with the hexahistidine (His) tag [76].

TALON® resin contains a tetradentate chelator charged with cobalt which has very high affinity to histidine, trapping proteins with a His tag to the stationary phase [77]. Elution of His-tagged proteins is achieved by addition of free imidazole, which competes with histidine and binds to the cobalt ion immobilized on the resin [76].

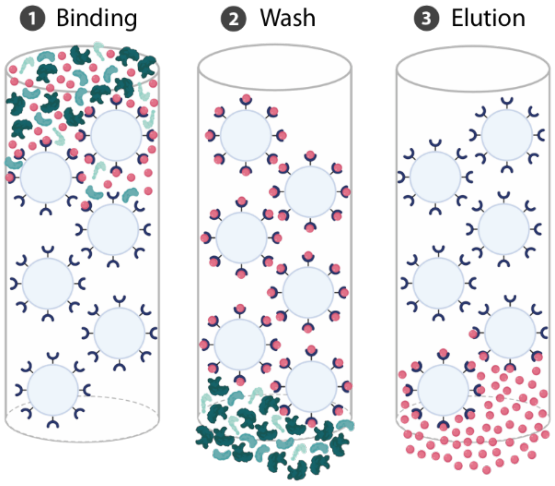

Figure 3-2 Affinity chromatography. The mobile phase contains the heterogeneous mixture and comes into contact with the stationary phase which comprises of a matrix or support material that holds the substrate covalently, while keeping groups required for target-binding exposed (1). Components in the mixture that have binding sites compatible with those in the immobilized substrate form reversible interactions that allow them to remain with the stationary phase during washing (2). All other components that do not interact with the immobilized substrate are readily washed out with the binding buffer and bound components can then be eluted out by adding a competing high-affinity ligand or by changing pH or polarity conditions (3). Figure illustrated using BioRender.

For this study, DNAJC12 and hTH1 were expressed as fusion proteins with a dual HisMBP tag. Both fusion proteins were purified via amylose affinity chromatography and the tags were removed using TEV protease that specifically recognizes the cleaving site located between the tags and the target protein. While DNAJC12 was isolated by trapping the His-TEV protease and the HisMBP tag with TALON® resin, hTH1 was isolated from the other cleavage components and products by size exclusion chromatography to avoid the replacement of the active site iron with cobalt [49].

3.5 Size Exclusion Chromatography

Unlike affinity chromatography which separates molecules based on their molecular interactions, size exclusion chromatography (SEC), also known as gel filtration chromatography, is a technique by which components of a mixture are separated by size [78] (Figure 3-3).

While SEC is a good tool for characterizing the oligomeric distributions of proteins, this method cannot be used to reliably determine molecular weight in all cases. Proteins with the same molecular weight but different shapes will interact differently with the pores and therefore result in varying retention volumes [78]. For instance, rod-shaped molecules will elute earlier than globular proteins of the same molecular weight [79]. The molecular weight of globular proteins, however, can be reliably estimated by SEC since they are widely used in standard calibration. Because nothing is known so far about the molecular shape of DNAJC12, SEC could not be used to absolutely determine its molecular weight.

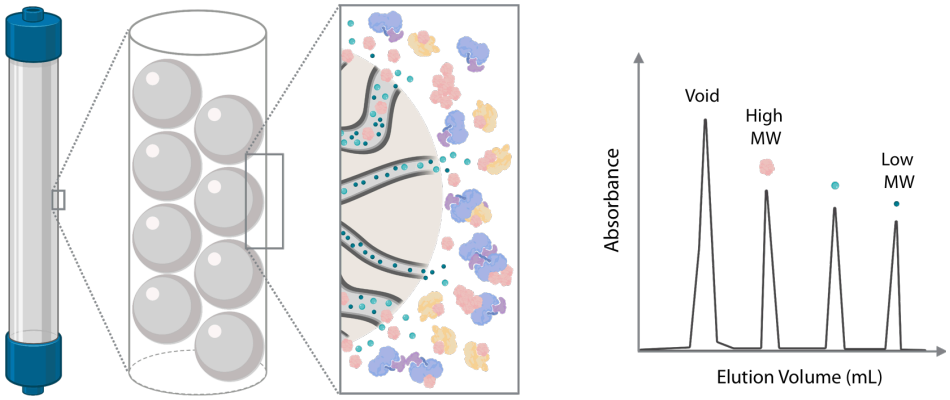

Figure 3-3 Size exclusion chromatography. The stationary phase consists of porous resin comprising of chemically inert, non-adsorptive spherical particle beads that are packed in a column. As the mobile phase carrying the heterogeneous mixture is added into the column, molecules that are larger than the pores do not diffuse into the beads, resulting in elution at the void volume. Molecules with sizes below the exclusion limit, which is defined as the maximum size of a molecule that can fit into the pores, can then be separated based on the degree of pore penetration. Larger molecules are unable to completely penetrate the pore, while molecules smaller than the smallest pores are able to and are thus eluted last. Illustration made with BioRender.

3.6 Dynamic Light Scattering

Dynamic light scattering (DLS), or photon correlation spectroscopy, is a non-destructive biophysical technique used to study properties and determine the size distribution of macromolecules by measuring their diffusion in solution. A monochromatic light beam or laser is directed to random-moving particles suspended in solution and a detector records the scattering intensity signal. As the light hits the moving particles, their random movement, also known as Brownian motion, causes a Doppler shift or a change in frequency and wavelength of light. The light scatters in different directions and the intensity scattering is measured by the detector which registers intensity fluctuations [80]. Larger particles result in less intensity fluctuations than those recorded for smaller particles. Intensity fluctuation measurements can then be analyzed to determine the diffusion coefficient that can then be used to determine the

hydrodynamic size of particles in solution. Since light hits particles at different orientations, the hydrodynamic size cannot be accurately estimated for non-spherical particles [80].

3.7 SEC coupled with Multi-angle Light Scattering

SEC coupled with multi-angle light scattering (SEC-MALS) is an absolute technique used to estimate the size of molecules in their native state using a combination of SEC and light scattering, allowing the analysis of the aggregation and oligomeric distribution of proteins. In this method, the components of a mixture are separated and eluted by size via SEC, which then pass through a multi-angle light scattering (MALS) and differential refractive index (dRI) detector. Similar to DLS, a laser is directed to the sample and the amount of light scattering is recorded by the MALS detector. The dRI detector measures the change in refractive index and is used to determine the concentration of the protein as it passes through the MALS detector. Both values are used to calculate the molecular weight of the sample. Should the sample be heterogeneous as it enters the detectors even after SEC, the calculated molecular weight will be an average of the molecules with the same elution volume [81].

3.8 Surface Plasmon Resonance

Surface Plasmon Resonance (SPR) is an optical technique that allows a label-free assessment of biomolecular interactions in real time. In this method, proteins are immobilized on a chip (ligand) while the putative binding partner remains in solution (analyte) [82] (Figure 3-4). For this study, immobilization was carried out by amine-coupling to a Biacore CM5 Chip, which has a gold surface with carboxymethylated dextran. N-hydroxysuccinimide is added to activate the carboxymethyl groups to form a highly reactive succinimide ester prior to the covalent binding of the ligand (the target protein; in this work this is the target protein TH). This reaction is followed by the addition of ethanolamine to block excess of activated esterified carboxyls [83].

A control is prepared similarly and is used by the SPR instrument as a reference surface during analysis. As the analyte (in this work DNAJC12) is injected to the chip, binding is assessed by measuring changes in the refractive index at the chip surface, which is recorded by the SPR instrument as an increased resonance signal [82]. By plotting the resonance signal as a function of time, a sensorgram graph can be derived which can graphically represent the

baseline, association and dissociation phases of the reaction. SPR technology not only allows the assessment of positive or negative binding, but also enables the determination of quantitative binding constants to evaluate binding affinity.

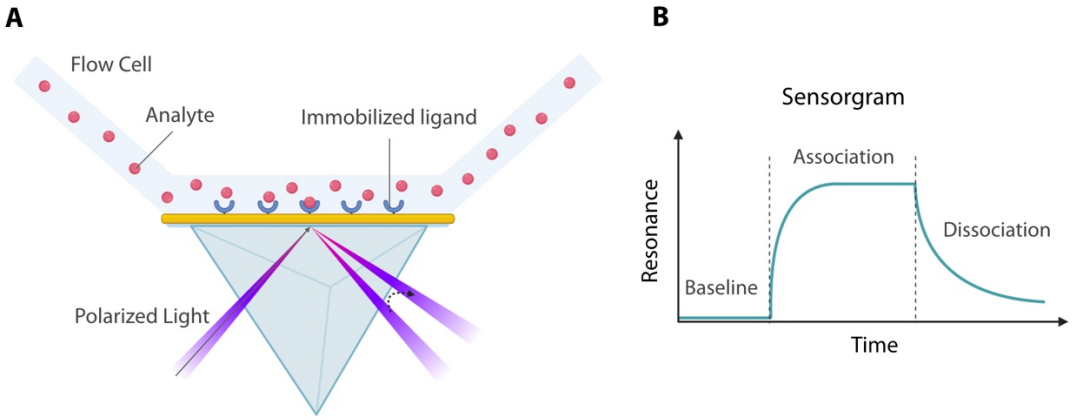

Figure 3-4 Surface plasmon resonance. (A) The ligand is immobilized on the chip and the analyte flows through the flow cell. Binding causes a shift in the refractive index at the chip surface resulting in the detection of an increased resonance signal as polarized light is directed to the chip. (B) The sample sensorgram shows the three phases of the binding reaction. The reaction begins at the baseline phase prior to analyte injection. Binding of the analyte to the ligand results in an increased resonance signal. Dissociation results in a decrease in resonance signal. Illustration made in BioRender and modified from [83].

4 Materials and Methods

Suppliers of chemicals and instruments, as well as catalog numbers for antibodies are provided in the text. For chemicals not specified, the supplier is Sigma-Aldrich.

4.1 *In silico* Homology Modelling and Structure Prediction

In silico homology modelling and structure predictions were carried out by submitting the amino acid sequence of DNAJC12 (UniProt Q9UKB3) into the Iterative Threading ASSEmbly Refinement (I-TASSER) [84] and the Protein DisOrder prediction System (PrDOS) programs [85].

4.2 Cloning of DNAJC12

All enzymes and nucleic acid kits used for cloning were provided by New England Biolabs.

4.2.1 Amplification of NcoI-*DNAJC12*-Acc65I

Polymerase chain reaction (PCR) was used to amplify the 573 bp *DNAJC12* cDNA from pUC-*DNAJC12* (a gift from Belén Pérez) using the forward primer DNAJC12-F (5'-GCTTCCATGGATGCAATTCTGAATT-3') and the reverse primer DNAJC12-R (5'-GCTTGGTACCTTAAATTTCATAATTACGA-3'). The primers were designed to introduce NcoI and Acc65I restriction sites flanking the 3' and 5' ends of the sequence, respectively (underlined). Amplification of the NcoI-*DNAJC12*-Acc65I fragment was obtained using OneTaq® Hot Start DNA polymerase with the thermal cycling conditions in Table 1.

Table 1 Thermal Cycling Conditions for Amplification of NcoI-DNAJC12-Acc65I.

Step	Temp. (°C)	Time	Cycles
Initial Denaturation	94	3 min	1
Denaturation	94	15 s	
Annealing	45	15 s	7
Extension	68	40 s	
Denaturation	94	20 s	
Annealing	58	30 s	25
Extension	68	40 s	
Final Extension	68	5 min	1
Hold	10	∞	1

4.2.2 Agarose Gel Electrophoresis

A 1% (w/v) agarose gel was prepared in Tris-acetate-EDTA (TAE) buffer (40 mM Tris, 20 mM acetate, 1 mM EDTA) and stained with GelRed™ Nucleic Acid Gel Stain (Biotium). GeneRuler 1kb DNA Ladder (Thermo Scientific) was used as a molecular weight ladder to quantitatively estimate the size of DNA. The agarose gel was run at 100 V for 45 min and visualized under UV light using the ChemiDoc XRS+ System.

4.2.3 Cloning of Human *DNAJC12* cDNA into Multiple Vectors

The three destination plasmid vectors pETMBP1a/*hTH1*, pETGST1a/*YFP* and pETZZ1a/*hTH1* were selected for cloning of the human *DNAJC12* cDNA [49, 72]. Simultaneous double digestions of the destination plasmids and the *DNAJC12* cDNA amplicons were done using NcoI and Acc65I FastDigest restriction enzymes at 37 ºC for 10 min. The digested plasmids were analyzed by agarose gel electrophoresis (Section 4.2.2) to separate the empty vectors from their current inserts.

The resulting 6455 bp, 6000 bp and 5724 bp fragments of pETMBP1a, pETGST1a and pETZZ1a vectors, respectively, were excised and subsequently purified using the Monarch® DNA Gel Extraction Kit and ligation of the cut gene amplicons into the empty purified vectors was carried out using T4 DNA Ligase with a 1:3 vector to insert ratio following the manufacturer's protocol. From each ligation reaction, 10 µl was used to chemically transform XL-10 Gold® Ultracompetent Cells (Agilent Technologies) by heat-shock treatment (30 min on ice, 30 s at 42 °C, 2 min on ice) and incubation at 37 °C for 1 h in SOC medium (2% tryptone, 0.5% yeast extract, 10 mM NaCl, 2.5 mM KCl, 10 mM $MgCl_2$, 10 mM MgSO4, 20 mM glucose). Positive transformants were selected by inoculating the samples onto Luria-Bertani (LB) agar plates supplemented with 50 µg/mL kanamycin (kan) and subsequently incubating them at 37 ºC overnight.

4.2.4 Colony PCR

Colony PCR was done to screen for colonies containing the plasmids with human *DNAJC12*. Five colonies were selected for each transformation and resuspended in nuclease-free water as template for the PCR reaction. Successful cloning of the *DNAJC12* cDNA was determined by the amplification of a 632 bp fragment using the DNAJC12-F and pETMBP-R

(5'-CGACGGAGCTCGAATTCGGATCC-3') primers. PCR was carried out using OneTaq® Hot Start DNA polymerase at the same thermal cycling conditions listed in Table 1, but with an additional two minutes for initial denaturation to lyse the bacterial cells. Screening results were analyzed by running the amplicons through a 1% w/v agarose gel in the same protocol previously described in Section 4.2.2.

4.2.5 Sequencing

Plasmid DNA was purified from colonies that showed positive results using the Monarch Plasmid Miniprep Kit following the manufacturer's protocol. Plasmid DNA concentrations were determined at A260 nm using the NanoDrop™ One Microvolume UV-Vis Spectrophotometer (Thermo Scientific). Sequencing reactions were prepared to each include 1 µL BigDye™ Terminator v3.1 Ready Reaction Mix (Applied Biosystems), 1 µL sequencing buffer, 300 ng plasmid DNA template, 3.2 µM primer and deionized water to a final reaction volume of 10 µL. The primers used in this experiment were DNAJC12-F, DNAJC12-R, pETMBP-F (5'- GACGCGCAGACTAATTCGGGATCT-3') and pETMBP-R. The thermal cycling (Table 2) was done and the samples were submitted to the DNA Sequencing Laboratory at Bergen High Technology Centre.

Table 2 Thermal Cycling Conditions for Samples for Sequencing.

Step	Temp. (°C)	Time	Cycles
Initial Denaturation	96	5 min	1
Denaturation	96	10 s	25
Annealing	50	5 s	
Extension	60	5 s	
Hold	10	∞	1

4.3 Expression and Purification of DNAJC12

4.3.1 Expression of HisMBP-DNAJC12

Plasmid DNA with the verified sequence of *DNAJC12* cDNA was used to transform BL-21 CodonPlus competent cells (Agilent Technologies). The cells were inoculated on LB agar plates containing 50 µg/mL kan and subsequently incubated at 37 ºC overnight to screen for positive transformants. Large-scale expression of HisMBP-DNAJC12 was carried out by

diluting a 25 mL overnight culture of bacteria harboring the pETMBP1a/*DNAJC12* plasmid in 500 mL of Terrific Broth (TB) or LB. Media was supplemented with 34 µg/mL chloramphenicol (cam) and 50 µg/mL kan. The cells were incubated at 37 ºC with a shaking frequency of 200 rpm until an optical density at 600 nm (OD_{600}) of 1.2-1.5 was reached for cultures grown in TB and 0.6-0.8 for those in LB. Protein expression was induced by the addition of either 0.5 mM or 1 mM IPTG and the cultures were incubated overnight at 28 ºC and 200 rpm. The cells were harvested by centrifugation at 4 ºC at 5000 xg for 20 min and the pellets were stored at -80 ºC.

4.3.2 Purification of HisMBP-DNAJC12

The cells were lysed by one round of freeze-thaw and subsequent sonication after resuspension in lysis buffer (20 mM Na-HEPES pH 7.0, 200 mM NaCl, 1X cOmplete™ Tablets (Roche), 10 mM benzamidine hydrochloride hydrate). The resuspended pellets were sonicated three times for 45 s (20 W output, 9-second pulses) using the Vibra-Cell™ Ultrasonic Liquid Processor (Sonics & Materials, Inc.) with 45-second pauses in between each round of sonication. The bacterial debris was removed by centrifugation for 20 min at 20000 xg at 4 ºC to obtain the crude extract.

The HisMBP-DNAJC12 fusion protein was purified by affinity chromatography at 4 ºC using amylose resin (New England Biolabs) on a gravity column. The resin was pre-equilibrated with binding buffer (20 mM Na-HEPES pH 7.0, 400 mM NaCl) and the crude extract was diluted 1:1 with the binding buffer before it was loaded onto the resin. The resin was washed with the binding buffer until the OD_{280nm} was below 0.10. The fusion protein was eluted using three column volumes (CV) of elution buffer (binding buffer with 10 mM maltose). To determine whether salt affects the yield of the purified fusion protein, initial tests for purification were performed using the MBPTrap™ 5 mL column (GE Healthcare) at 4 ºC at a flow rate of 2 mL/min using buffers supplemented with either 200 mM or 400 mM NaCl.

Fractions containing protein were pooled and concentrated using Amicon® Ultra-15 (50 kDa MWCO) centrifugal filters (Merck-Millipore) by centrifugation at 3900 xg at 4 ºC for 30 to 60 min. Protein concentration was determined at 280 nm using the NanoDrop™ One Microvolume UV-Vis Spectrophotometer using the theoretical extinction coefficient (ε) of

1.55 (1 mg/mL) [86]. Sodium dodecyl sulfate polyacrylamide gel electrophoresis (SDS-PAGE) was used to check the purity of the fusion protein (Section 4.5).

4.3.3 Isolation of DNAJC12

The purified fusion protein was cleaved by TEV protease using a 1:5, 1:10, 1:50 or 1:100 protease to fusion protein ratio (w/w) and incubation at 35 °C for at least 60 min. TEV protease and HisMBP tag were removed from the cut sample by IMAC using TALON® resin (Takara Bio) on a gravity column. The resin was equilibrated with three CV of binding buffer before sample loading. The sample was incubated with the resin at room temperature for 20 min with light shaking. The flow-through was then collected, reloaded and incubated with the resin for another 20 min. Finally, the flow-through and three CV of binding buffer were collected again and concentrated using the Amicon® Ultra-15 centrifugal filters (Merck-Millipore) with 10 kDa MWCO by centrifugation at 3900 xg at 4 ºC for 30 to 60 min. Protein concentration was determined at 280 nm using the theoretical extinction coefficient (ε) of 1.50 (1 mg/mL) [86]. The results of the purification were analyzed by SDS-PAGE (Section 4.5).

4.4 Expression and Purification of human tyrosine hydroxylase 1 (hTH1)

The recombinant expression of hTH1 was obtained in a similar protocol as described in Section 4.3.1, but with BL-21 CodonPlus competent cells with the pETMBP1a*/hTH1* grown in LB broth and the addition of 0.25 mM ferrous ammonium sulfate at the time of induction. Cell lysis, sonication and protein purification were done as previously described in Section 4.3.2, but with 200 mM NaCl in the buffer and supplementation of the lysis buffer with 1X cOmplete™ EDTA-Free Protease Tablets (Roche). Protein concentration was determined at 280 nm using the theoretical extinction coefficient (ε) of 11 (1 mg/mL) [86].

The purified HisMBP-hTH1 fusion protein was cleaved by a His-tagged TEV protease [87] using a 1:10 protease to fusion protein ratio (w/w) and incubation at 4 °C for 60 to 120 min. The hTH1 protein was isolated from TEV protease and HisMBP by preparative size exclusion chromatography (SEC) using the HiLoad™ 16/60 Superdex™ 200 PG column (GE Healthcare) connected to the ÄKTA™ Pure Protein Purification System (GE Healthcare) at 4 °C with a 0.40 mL/min flow rate. Fractions of 500 µl were collected, and those corresponding to the hTH1 peak on the chromatogram were pooled and concentrated using Amicon® Ultra-

15 (50 kDa MWCO) centrifugal filters by centrifugation at 3900 xg at at 4 ºC for 30 to 60 min. Protein concentration was determined at A280 nm using the theoretical extinction coefficient (ε) of 7.3 (1 mg/mL) calculated from the hTH1 protein sequence [86].

4.5 Sodium dodecyl sulfate Polyacrylamide Gel Electrophoresis

SDS-PAGE was carried out by denaturing the protein samples via the addition of an equal volume of 2X Laemmli sample buffer (Bio-Rad) with a final concentration of 100 µM DTT followed by heating at 95 °C for 5 min before loading into a 10% Mini-PROTEAN® TGX™ Precast Protein Gel (Bio-Rad) and run at 300 V for 20 min using SDS-PAGE running buffer (25 mM Tris, 200 mM glycine, 0.1% SDS). The Precision Plus™ Dual Color Standard (Bio-Rad) was used as a molecular weight ladder. The gel was stained using Coomassie (0.08 mM Coomassie brilliant blue G-250 (Bio-Rad), 5 mM HCl), destained in water and imaged using the ChemiDoc XRS+ System (Bio-Rad).

4.6 Western Blot

Samples were analyzed by SDS-PAGE (Section 4.5) and blotted onto a PVDF membrane using the PVDF Transblot Transfer Pack and the Trans-Blot® Turbo™ Transfer System (Bio-Rad) following the manufacturer's instructions. The membranes that were stained with Coomassie were incubated in methanol until the stain was no longer visible, and then washed with acetic acid for 5 min to remove excess methanol.

The membranes were then washed with washing buffer (20 mM Tris, 140 mM NaCl, 0.1% Tween® 20 pH 7.4) for 5 min three times with gentle agitation before blocking with 5% whole milk for 1 h followed by incubation with the primary antibodies rabbit anti-DNAJC12 C-terminus (1:5000; ABCAM, cat# AB167425), rabbit anti-DNAJC12 N-terminus (1:5000; LS BioSciences, Inc., cat# LS-C463669) or rabbit anti-totalTH (1:5000; Thermo Fisher Scientific, cat# OPA1-04050) for 45 min. Unbound primary antibodies were removed by washing before incubation of the membrane with the secondary antibody goat anti-rabbit pAb conjugated to horse radish peroxidase (1:1000; Bio-Rad, cat#170-6515). Luminita Immobilon Crescendo Western HRP substrate (Merck Millipore) was added to the membrane prior to visualization using the ChemiDoc™ XRS+ System. When required, blots were stripped with Re-blot Plus Strong stripping buffer (Temecula California) before re-probing.

4.7 Size Exclusion Chromatography

4.7.1 Analytical SEC

Analytical SEC was done using Superose™ 6 Increase 10/300 GL, Superdex™ 200 Increase 10/300 GL or Superdex™ 75 10/300 GL columns (GE Healthcare) connected to the ÄKTA™ Pure Protein Purification System. Analysis of 100 µg (at 1 mg/ml) samples was performed at 4 ºC at a flow rate of either 0.50 or 0.75 mL/min after pre-equilibration of the column with buffer. Samples that required lower salt concentrations than the purification buffer were buffer exchanged using the Zeba™ Spin Desalting Column (Thermo Scientific) following the manufacturer's instructions. Column calibration was done with the Low Molecular Weight (LMW) Gel Filtration Calibration Kit (GE Healthcare). The Superdex™ 200 Increase 10/300 GL column was also used at 0.40 mL/min to collect 250 µl fractions for analysis of peak contents by SDS-PAGE (Section 4.5). For initial binding studies, 100 µg of DNAJC12 and 100 µg of hTH1 were incubated at 4 ºC for 10 min prior to SEC, while 1 mg of DNAJC12 and 1 mg of hTH1 was used for cryogenic electron microscopy (Cryo-EM) sample preparation.

4.7.2 SEC coupled with Multi-angle Light Scattering

SEC-MALS was carried out using a Superdex™ 200 Increase 10/300 GL connected to the ÄKTA™ Purifier FPLC system (GE Healthcare), which was coupled to a RefractoMax 520 module (ERC, Inc.) and mini-DAWN TREOS detector (Wyatt). The column was equilibrated with 20 mM Na-HEPES pH 7.0, 200 mM NaCl prior to sample analysis at a flow rate of 0.40 mL/min. For binding studies, a sample containing 20 µM of hTH1 and 40 µM of DNAJC12 (pre-incubated at 4 ºC for 10 min) was used for the experiment and another sample containing only 20 µM hTH1 was used as a control. Sample molar masses were estimated using the Astra software (Wyatt).

4.8 Dynamic Light Scattering

Dynamic light scattering (DLS) using the Zetasizer Nano ZS instrument (Malvern Panalytical) was done to estimate the hydrodynamic size of the protein samples. Light scattering was measured using a He-Ne laser at 683 nm with a fixed scattering angle of 173° at 37 °C and data analysis was conducted on the intensity and volume size distribution curves, as well as the Z-average values using the Zetasizer software (Malvern).

For experiments on the analysis of DNAJC12 oligomeric distribution, 40 µM (subunit) samples were analyzed in 20 mM Na-HEPES pH 7.0 buffer without or with 400 mM NaCl. For binding studies, hTH1 and DNAJC12 were analyzed at 10 µM (subunit) and 20 µM (subunit), respectively, in 20 mM Na-HEPES pH 7.0, 200 mM NaCl buffer. The control sample contained 10 µM (subunit) of hTH1 and the measurements were recorded every 3 min for 120 min. Data from three replicates were analyzed using the Prism 8 software (GraphPad).

4.9 Surface Plasmon Resonance

SPR was carried out to verify binding of DNAJC12 and hTH1, as well as to determine the equilibrium dissociation constant (K_D) of the reaction. Salt was removed from the hTH1 preparation using the Zeba™ Spin Desalting Column following the manufacturer's instructions. SPR was performed using the Biacore T200 instrument (GE Healthcare) and a Series S CM5 chip (GE Healthcare). Immobilization of hTH1 on the chip was obtained by carboxymethyl activation using N-hydroxysuccinimide and amide linkaging using ethanolamine. hTH1 was diluted in 10 mM sodium acetate pH 5.0 buffer (GE Healthcare) and injected until a signal of approximately 10 000 response units (RU) was reached.

A solution containing 10 mM DTT was injected and HBS-N buffer (GE Healthcare; 10 mM Na-HEPES pH 7.4, 150 mM NaCl) was used to wash the unbound hTH1 molecules. HBS-N buffer was also used as both running and analyte binding buffer. The purified DNAJC12 preparation was injected unto the chip at different concentrations (100 nM, 200 nM, 400 nM, 800 nM, 1600 nM, 2400 nM, 3200 nM) and allowed to interact with the immobilized hTH1 for a total contact time of 140 s. Bound DNAJC12 species were removed by washing with HBS-N buffer for 600 s before moving on to the next concentration. The resulting sensorgrams were analyzed and the K_D values were estimated using the Biacore evaluation software (GE Healthcare).

4.10 Tandem Mass Spectrometry

Samples were analyzed by SDS-PAGE (Section 4.5) and the bands-of-interest were excised and submitted to the Proteomics Unit at the University of Bergen (PROBE) for MS/MS analysis to verify ubiquitination and identify the ubiquitinated residue/s. The results were analyzed using the Scaffold 4 software (Proteome).

4.11 Statistical Analysis

Measurements were repeated five times for experiments on the effect of varying NaCl concentrations on DNAJC12 oligomerization, while experiments on monitoring of hTH1 aggregation by DLS were repeated three times. The estimated hydrodynamic diameters and Z-average values of the samples from individual measurements obtained by DLS were analyzed by Excel (Microsoft) and Prism 8 (GraphPad) to determine and plot the standard deviation (SD).

In the SPR experiments, the standard error of mean (SEM) of the K_D values from the four individual sensorgrams as well as for the concentration for half-maximal binding of DNAJC12 (EC_{50}) calculated from the fitting of the concentration dependent response units (RU) to a Langmuir equation (hyperbolic equation) were obtained by Prism 8 (GraphPad).

5 Results

5.1 *In silico* – based Homology Modelling and Structure Prediction

In order to gain insights into the structure of DNAJC12, its amino acid sequence was submitted to the PrDOS program which predicts the probability of disorder and the I-TASSER program which predicts protein structure by iterative template-based modelling. Results from PrDOS showed that DNAJC12 J-domain region (residues 14-79) is, as expected, structured while the rest of the protein is more likely to be disordered (Figure 5-1A). Analysis by I-TASSER resulted in five potential structures and the model that fit best with the PrDOS results is shown in Figure 5-1B.

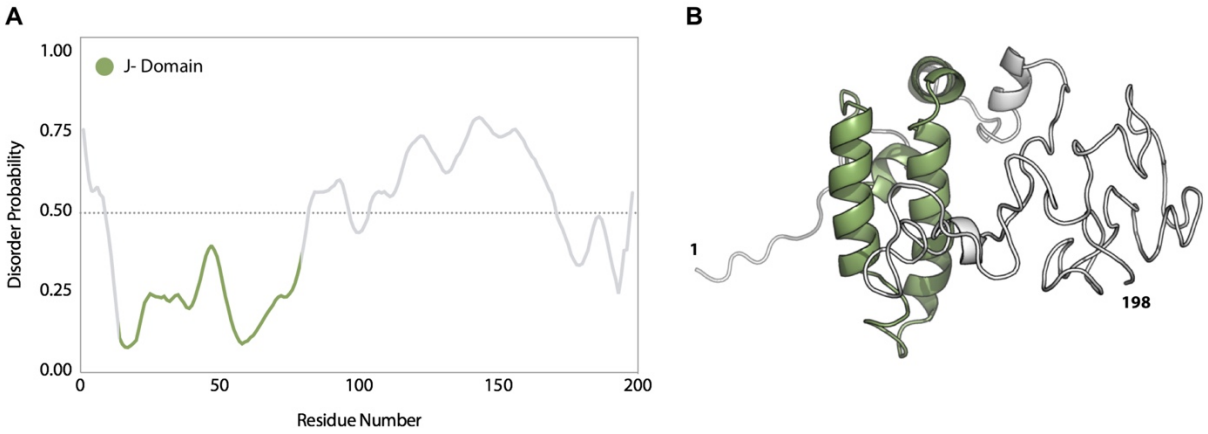

Figure 5-1 Results from *in silico*- based homology modelling and structure prediction software PrDOS and I-TASSER. (A) Prediction of disordered regions by PrDOS. The disorder threshold (at 0.5 probability) is shown by the dotted line. (B) One of the DNAJC12 structures predicted by I-TASSER. The J-domain (residues 14-79) is highlighted in green.

5.2 Cloning of DNAJC12

The human *DNAJC12* cDNA was cloned into three destination plasmids using restriction enzyme cloning. Five bacterial colonies for each type of vector were analyzed by PCR to find colonies with plasmids where *DNAJC12* had been successfully incorporated into the vector. Only ten colonies were tested (5 each for pETMBP1a and pETGST1a vectors) because no transformants were obtained for pETZZ1a.

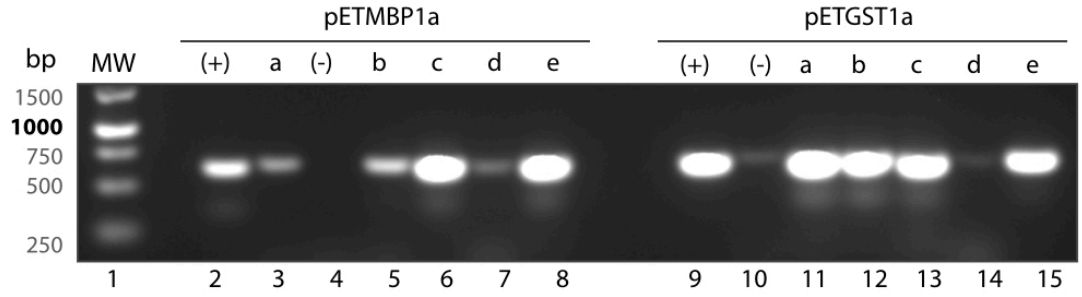

Figure 5-2 Colony screening for selection of pETMBP1a/*DNAJC12* and pETGST1a/*DNAJC12* using PCR. Lane 1: GeneRuler 1kb DNA ladder; lanes 2 and 9: DNAJC12 positive controls; lanes 4 and 10: negative controls (using pETMBP1a/*hTH1* and pETGST1a/*YFP* as templates); lanes 3,5-8 and lanes 11-15: PCR amplicons from five transformed colonies with the putatitive pETMBP1a/*DNAJC12* and pETGST1a/*DNAJC12* vector.

A band of approximately 600 bp was obtained for all ten colonies, consistent with the expected size of the amplicon which is 632 bp (Figure 5-2). Plasmids from the six colonies that gave the strongest bands (MBPc, MBPe, GSTa, GSTb, GSTc, GSTe) were sequenced to verify the absence of mutations and that *DNAJC12* was placed in correct reading frame with the fusion partners. Three of the six colonies (MBPc, MBPe, GSTc) had plasmids with the correct DNAJC12 sequence in the correct reading frame while GSTa, GSTb and GSTe presented mutations that would result in missense mutations. While we now have plasmids to correctly express both HisMBP-DNAJC12 and HisGST-DNAJC12, DNAJC12 encoded by pETMBP1a/*DNAJC12* was selected for all downstream experiments in this work (Figure 5-3).

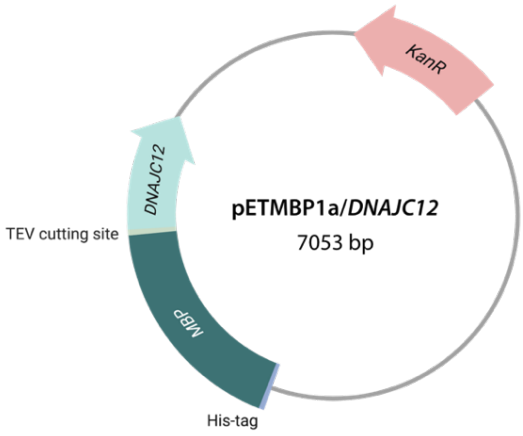

Figure 5-3 Simplified pETMBP1a/*DNAJC12* plasmid map. Human *DNAJC12* cDNA was cloned at the C-terminus of HisMBP. The open reading frames for HisMBP-DNAJC12 fusion protein and kanamycin resistance (*KanR*) are shown as arrows. The TEV protease cleavage site is also indicated on the map.

5.3 Expression and purification of the Fusion protein HisMBP-DNAJC12

BL-21 CodonPlus competent cells were transformed with the pETMBP1a*/DNAJC12* plasmid and positive transformants were selected by antibiotic selection. The transformants were then grown in LB and successful expression of HisMBP-DNAJC12 was obtained by inducing with either 0.5 mM or 1 mM IPTG, as denoted by a strong band on SDS-PAGE with a size of 67 kDa. (Figure 5-4A).

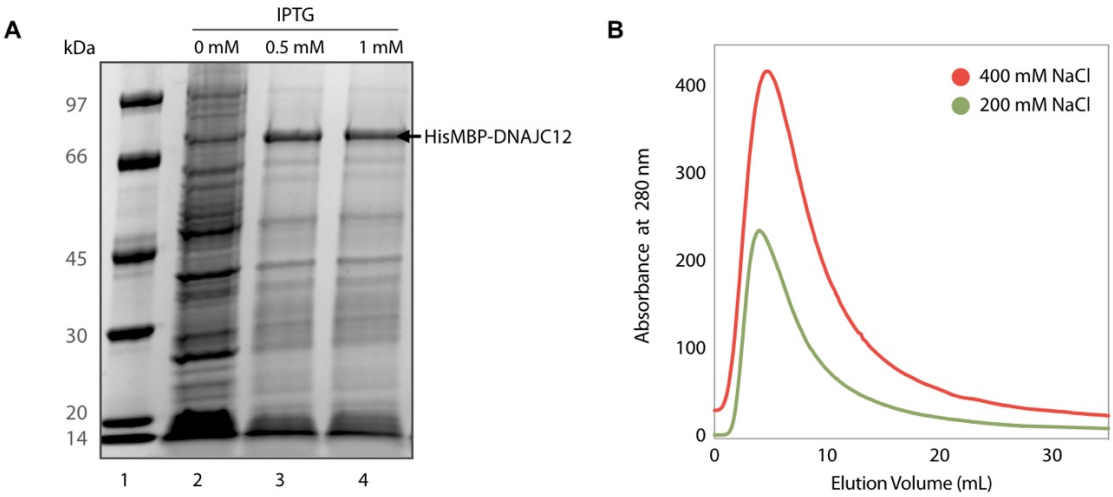

Figure 5-4 Expression and purification of HisMBP-DNAJC12. (A) SDS-PAGE showing the induction of HisMBP-DNAJC12 by IPTG. Lane 1: Precision Plus™ Dual Color ladder; lane 2: uninduced control sample; lanes 3 and 4: samples from cultures induced with either 0.5 mM or 1 mM IPTG. (B) Elution profiles from the initial amylose affinity chromatography tests of HisMBP-DNAJC12 using 400 mM salt in the buffer (red) or 200 mM salt in the buffer (green) analyzed using an MBPTrap™ 5mL column at 4 °C at a 2 mL/min flow rate.

The cells were collected and lysed, and HisMBP-DNAJC12 was separated from bacterial proteins using amylose affinity chromatography. The initial purification was carried out using 20 mM Na-HEPES pH 7.0 buffer supplemented with 200 mM NaCl with a yield of 2.3 mg/L culture. The second purification trial was done in the same buffer but with 400 mM NaCl, which led to a two-fold increase in yield to 4.8 mg/L (Figure 5-4B). In an attempt to further optimize the yield of fusion protein, the transformants were grown in Terrific Broth (TB) which resulted in increased yield by six-fold compared to LB and was chosen as standard. The purity of HisMBP-DNAJC12 was then analyzed on SDS-PAGE, which resulted in a single band at approximately 67 kDa. (Figure 5-5A).

5.4 Purification of DNAJC12

His-tagged TEV protease was expressed and purified following a protocol previously established in the laboratory, resulting in a yield of ~20 mg/L culture. The cutting of HisMBP-DNAJC12 was optimized to determine the amount of time and TEV protease necessary to cleave fusion protein efficiently. As observed by denaturing SDS-PAGE (Figure 5-5A), incubation of HisMBP-DNAJC12 with TEV protease in varying TEV:fusion protein ratios resulted in a decreased amount of fusion protein (67 kDa) and increased amounts of both HisMBP and DNAJC12, denoting successful cleavage of the fusion protein. In the gel, HisMBP and DNAJC12 are observed as bands at 44 kDa and 27 kDa respectively, consistent with their theoretical molecular weights (43 kDa; 24 kDa). In the 1:5 and 1:10 reactions, a band corresponding to TEV protease (27 kDa) is seen just below DNAJC12.

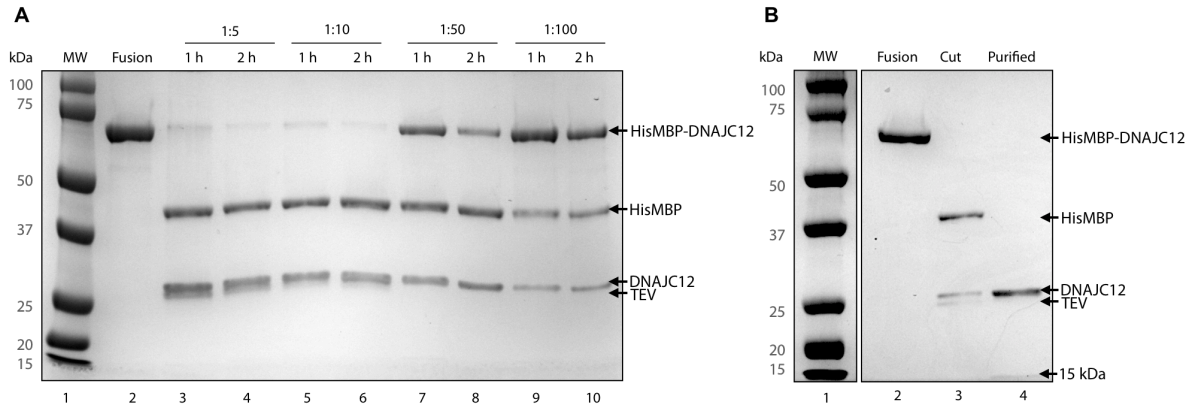

Figure 5-5 Isolation of DNAJC12. Denaturing SDS-PAGE showing (A) HisMBP-DNAJC12 cutting using varying amounts of TEV protease. Lane 1: Precision Plus™ Dual Color Standard, lane 2: HisMBP-DNAJC12 fusion protein, lanes 3-10: HisMBP-DNAJC12 cut with different TEV:fusion protein ratios incubated at 35 °C for either 1 or 2 h. (B) Purification of DNAJC12. Lane 1: Precision Plus™ Dual Color Standard, lane 2: His-MBP-DNAJC12, lane 3: HisMBP-DNAJC12 incubated in 1:10 ratio at 35 °C for 1 h, lane 4: purified DNAJC12.

Incubation of the protein with TEV protease at 1:50 and 1:100 ratios resulted in incomplete cleavage of the fusion protein even after 2 hours, while almost all fusion protein was cleaved in the 1:5 and 1:10 reactions within the first hour. The resistance of some fusion protein to cleavage may indicate inaccessibility of TEV protease due to aggregated fusion proteins. Nevertheless, incubation of the fusion protein with TEV-protease at a 1:10 ratio (TEV:fusion protein) for 1 hour at 35 °C was chosen. DNAJC12 was subsequently isolated from TEV protease, HisMBP-DNAJC12 and HisMBP by IMAC using TALON® resin. As

observed from Figure 5-5B (lane 4), the purified sample yielded a strong band with a size of approximately 27 kDa and a faint band at ~15 kDa.

5.5 Expression and Purification of Human Tyrosine Hydroxylase 1 (hTH1)

BL-21 CodonPlus competent cells with the pETMBP1a/*hTH1* plasmid were grown in LB and protein expression was induced by 0.5 mM IPTG. HisMBP-hTH1 was purified by amylose affinity chromatography on a gravity column and subsequently cleaved using a 1:10 TEV protease to fusion protein ratio. Successful purification of the fusion protein was determined by denaturing SDS-PAGE and was observed as a strong band at approximately 100 kDa, consistent with the theoretical MW of the protein (99 kDa; Figure 5-6B). Cleavage with TEV protease (27 kDa) resulted in two bands corresponding to HisMBP (43 kDa) and hTH1 (~60 kDa band; 56 kDa MW) [49]. Tetrameric hTH1 was isolated by SEC, which was collected at an elution volume of 60.7 mL, resulting in a yield of 1.4 mg per 1 L of culture [49] (Figure 5-6A). hTH1 was isolated after SEC, shown as a strong 60 kDa band on SDS-PAGE (Figure 5-6B).

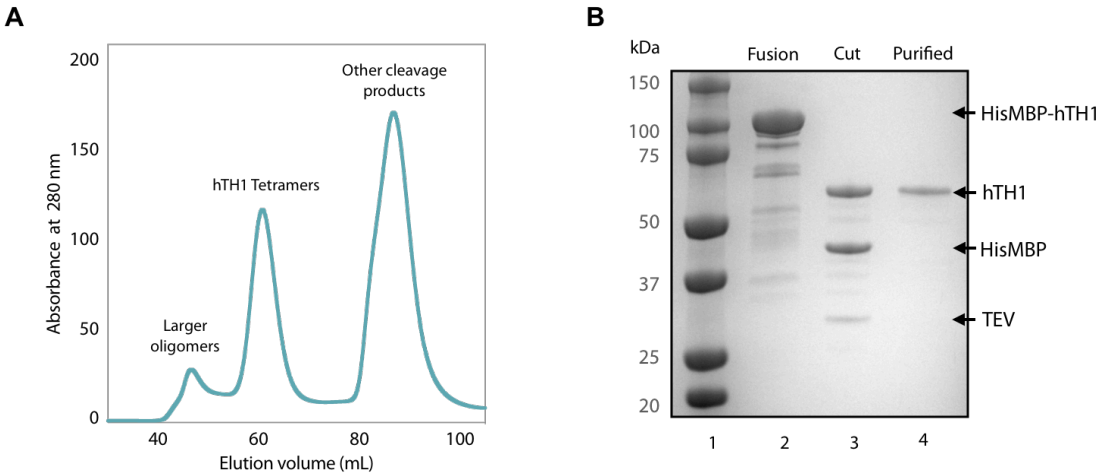

Figure 5-6 Purification of hTH1. (A) SEC of the cut fusion protein HisMBP-hTH1 (7 mg). SEC profile shows the separation of large oligomers, tetramers and a mixture of HisMBP and TEV protease on a HiLoad™ 16/60 Superdex™ 200 PG column at 4 °C at 0.40 mL/min flow rate. [49] (B) Denaturing SDS-PAGE of the purification of hTH1. Lane 1: Precision Plus™ Dual Color Standard, lane 2: HisMBP-hTH1 fusion protein, lane 3: cut sample, lane 4: purified hTH1.

5.6 Analysis of Purity and Oligomeric Distribution of DNAJC12

Initial SEC analyses of the purified DNAJC12 sample were performed both to evaluate the oligomeric distribution of the sample and – combined with SDS-PAGE and western blot

analyses – the degree of purity. Analyses by denaturing SDS-PAGE and subsequent western blot allow the investigation of purity by showing contaminations by subunit size, while SEC shows the oligomeric organization of the protein in native conditions.

The SEC profile from a Superose™ 6 column showed two major peaks indicating the presence of two forms of DNAJC12. These peaks eluted at high elution volumes, suggesting that SEC should be repeated using a column with a smaller size range (Figure 5-7A). Further analysis of the sample in higher resolution using Superdex™ 200 and Superdex™ 75 columns indicated the presence of three forms of DNAJC12 (Peaks 1, 2 and 3 (P1, P2 and P3) in Figure 5-7B;C). The analysis also revealed that the three forms of DNAJC12 could be separated from larger aggregates even in the Superdex™ 75 column, which has the smallest size range.

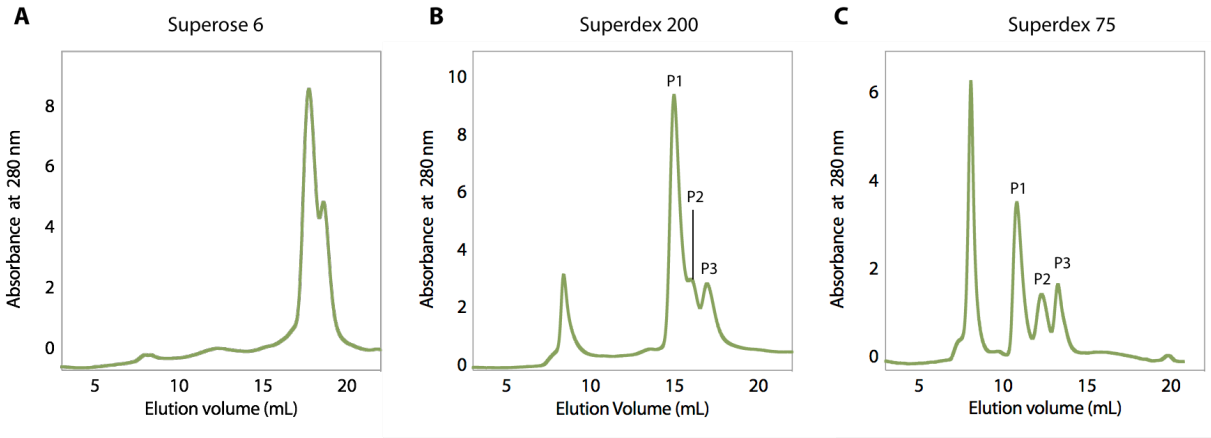

Figure 5-7 Analytical SEC of DNAJC12 using multiple columns with increasing resolution. Analysis of purified DNAJC12 (100 µg at 1 mg/mL) on the Superose™ 6 (A) Superdex™ 200 (B) and Superdex™ 75 (C) Increase 10/300 GL columns using 20 mM Na-HEPES pH 7.0 buffer with 400 mM NaCl at 4 °C at a flow rate of 0.50 mL/min.

The molecular weights of species in each peak were estimated based on a calibration curve obtained using the Gel Filtration Calibration Kit (LMW) (Figure 5-8B; inset). Because the three peaks were not completely resolved using the Superdex™ 200 column, only the chromatogram obtained from the Superdex™ 75 column (Figure 5-7C) was used to estimate the sizes of the three species.

The gel phase distribution coefficients (K_{av}) of each peak were calculated using the equation $K_{av}=(V_e-V_0)/(V_t-V_0)$, where V_e is the elution volume, V_0 is the void volume (8.1 mL), and V_t is the total bed volume (24 mL). The V_0 value was determined by running blue dextran through the column. The K_{av} values of the three peaks were determined to be 0.17, 0.26 and

0.32 for P1, P2 and P3 respectively. These K_{av} values were used to estimate the sizes of the species eluting out at each peak from the derived calibration curve equation (y=-0.4108x+2.089). Proteins eluting out at the P1, representing the largest population, were estimated to be ~47 kDa, which is in the range of a DNAJC12 dimer. Species in P2 were estimated to be ~28 kDa, which is close to the expected molecular weight of a DNAJC12 monomer. Proteins that elute out at P3 were estimated to have molecular weights of approximately 20 kDa, which is consistent with the observed ~15 kDa band in the purified sample analyzed by denaturing SDS-PAGE (Figure 5-8A).

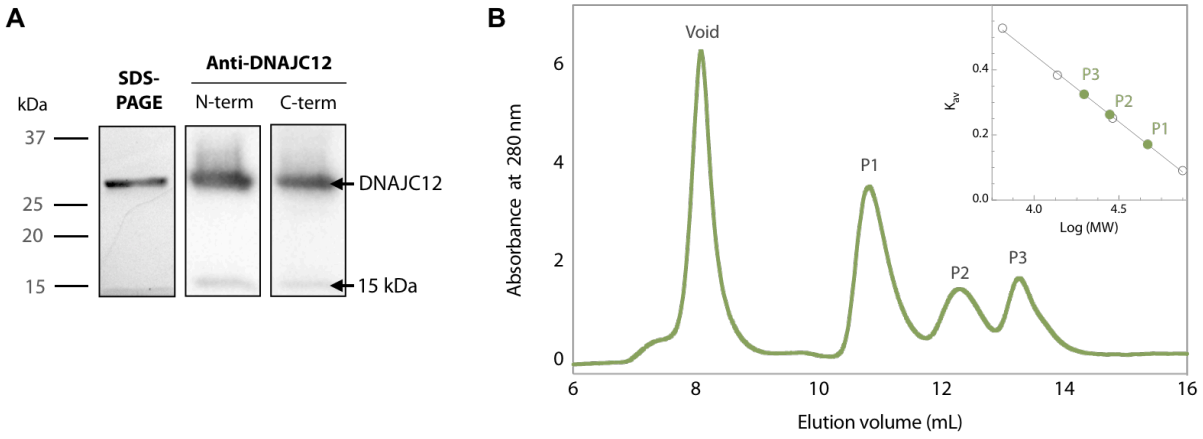

Figure 5-8 Analysis of purified DNAJC12 by denaturing SDS-PAGE, western blot and native SEC. (A) SDS-PAGE and western blot analyses using antibodies against the N- or C- terminus of the protein on the purified DNAJC12 sample. The Precision Plus™ Dual Color Standard was used as a molecular weight ladder. (B) A calibration curve was derived via the analysis of conalbumin (75 kDa), carbonic anhydrase (29 kDa), ribonuclease A (13.7 kDa) and aprotinin (6.5 kDa) on a Superdex™ 75 10/300 GL column at 0.50 mL/min (inset). The linear equation y = -0.4108x+2.089 was derived from the curve with an r^2 value of 0.999. Species eluting at P1, P2 and P3 were estimated to be approximately 47 kDa, 28 kDa and 20 kDa respectively.

Further investigation of the purified DNAJC12 sample was carried out by western blot (following denaturing SDS-PAGE) using antibodies that recognized epitopes at the N-terminus and C-terminus of the protein. DNAJC12 was detected, as expected, in the 27 kDa band corresponding to the full-length DNAJC12 (24 kDa), confirming that purified DNAJC12 has a decreased relative mobility resulting in a higher apparent molecular weight on SDS-PAGE and western blot (Figure 5-8A). A faint ~15 kDa band was also detected in the purified protein sample using both antibodies indicating degraded forms of both N-terminal and C-terminal halves of DNAJC12.

5.7 Effect of Salt on the Oligomeric Distribution of DNAJC12

5.7.1 Dynamic Light Scattering (DLS) Analysis

DLS was used as an initial method to determine the effect of removing salt from the buffer on the native oligomeric distribution of purified DNAJC12 (Figure 5-9). Purified DNAJC12 suspended in buffer supplemented with 400 mM NaCl consists mostly of a population with an apparent hydrodynamic diameter of 7.0 ± 0.89(SD) nm. Desalting of the buffer resulted in an increased apparent hydrodynamic diameter to 27.4 ± 6.82(SD) nm suggesting the formation of larger molecules and thus the alteration of oligomeric distribution of recombinant DNAJC12 in the absence of salt *in vitro*. Because the sample is not homogenous, these results were only used as indications of altered oligomeric distribution, and not to quantitatively determine the hydrodynamic size of the protein.

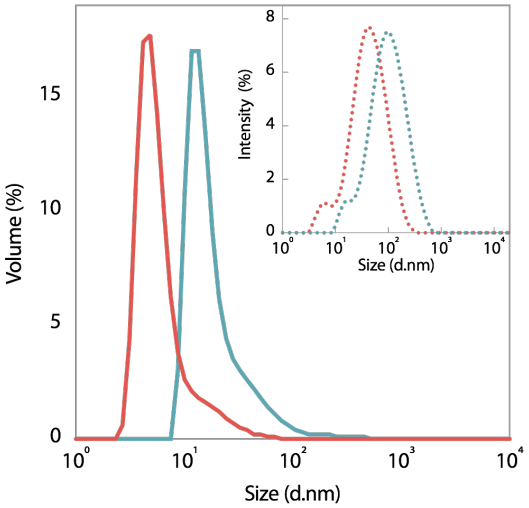

Figure 5-9 Initial analysis of purified DNAJC12 oligomeric distribution by DLS. Size distribution of DNAJC12 by volume (solid line) and by intensity (dotted line; inset) in 400 mM (red) and 0 mM (blue) NaCl buffers at 37 °C. The data represents the mean of five measurements.

5.7.2 Size Exclusion Chromatography (SEC) Analysis

Analytical SEC using a Superose™ 6 column of purified DNAJC12 in 20 mM Na-HEPES buffer pH 7.0 without and with NaCl at different concentrations (200 mM, 400 mM NaCl) was done in parallel with the DLS experiment to verify the effect of salt on the native DNAJC12 oligomeric distribution. As observed in Figure 5-10, purified DNAJC12 mostly eluted between 15-20 mL in 200 mM and 400 mM salt buffers.

However, when it was suspended in buffer without salt, DNAJC12 was mostly observed as larger oligomers or aggregates in the void volume or between 10-15 mL. While slightly more of the DNAJC12 aggregates were observed in the 200 mM sample compared to those in 400 mM NaCl, this decrease in salt concentration did not significantly alter its oligomeric distribution. The buffer supplemented with 200 mM salt, better representing physiological conditions, was therefore selected in the succeeding experiments.

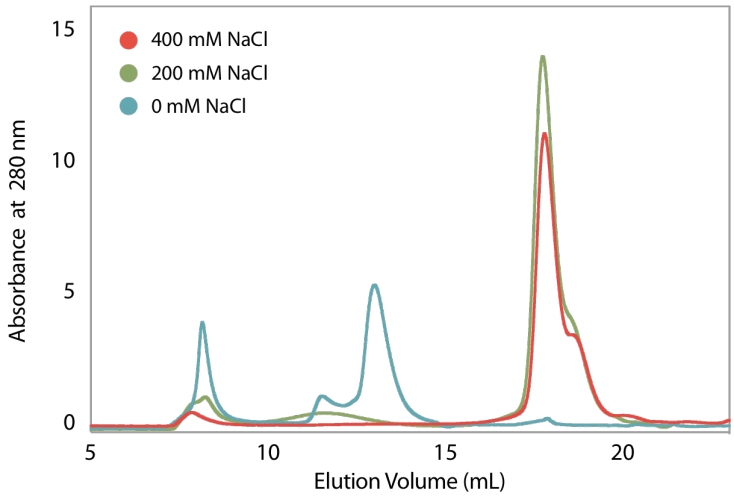

Figure 5-10 Analytical SEC of purified DNAJC12 in buffers with varying NaCl concentrations. SEC analysis of purified DNAJC12 preparations (100 µg) in 20 mM Na-HEPES pH 7.0 buffer without NaCl (blue), 200 mM NaCl (green), and 400 mM NaCl (red) using a Superose™ 6 10/300 Increase GL Column at 4 °C at a flow rate of 0.50 mL/min.

5.8 Binding of hTH1 and DNAJC12

5.8.1 Size Exclusion Chromatography (SEC) Analysis

Analytical SEC, using a Superdex™ 200 Increase 10/300 GL column, was carried out to determine whether hTH1 and DNAJC12 interacted *in vitro*. The two proteins were incubated together for 5-10 min at 4 °C prior to SEC analysis.

As observed in Figure 5-11, the tetrameric hTH1 peak, which originally eluted out at 10.8 mL in the control sample, shifted to 10.6 mL in the sample with DNAJC12. The DNAJC12 peak eluting at 15.1 mL (Figure 5-11B;C) containing the apparent dimer (P1 from Figure 5-8B) was significantly decreased in the binding sample as compared to the DNAJC12 control. This decrease, together with the apparent increase in size of hTH1 in the binding sample, strongly indicated that the two proteins co-elute and that the form of DNAJC12 eluting at 15.1 mL is the one that associates to hTH1 (Figure 5-11B-D). Fractions containing the

possible complex of hTH1-DNAJC12 were collected and analyzed by SDS-PAGE. Indeed, hTH1 and DNAJC12 were the major content of the fraction represented by bands at ~60 kDa and ~27 kDa, respectively (Figure 5-11E). Some degradation of hTH1 was also observed.

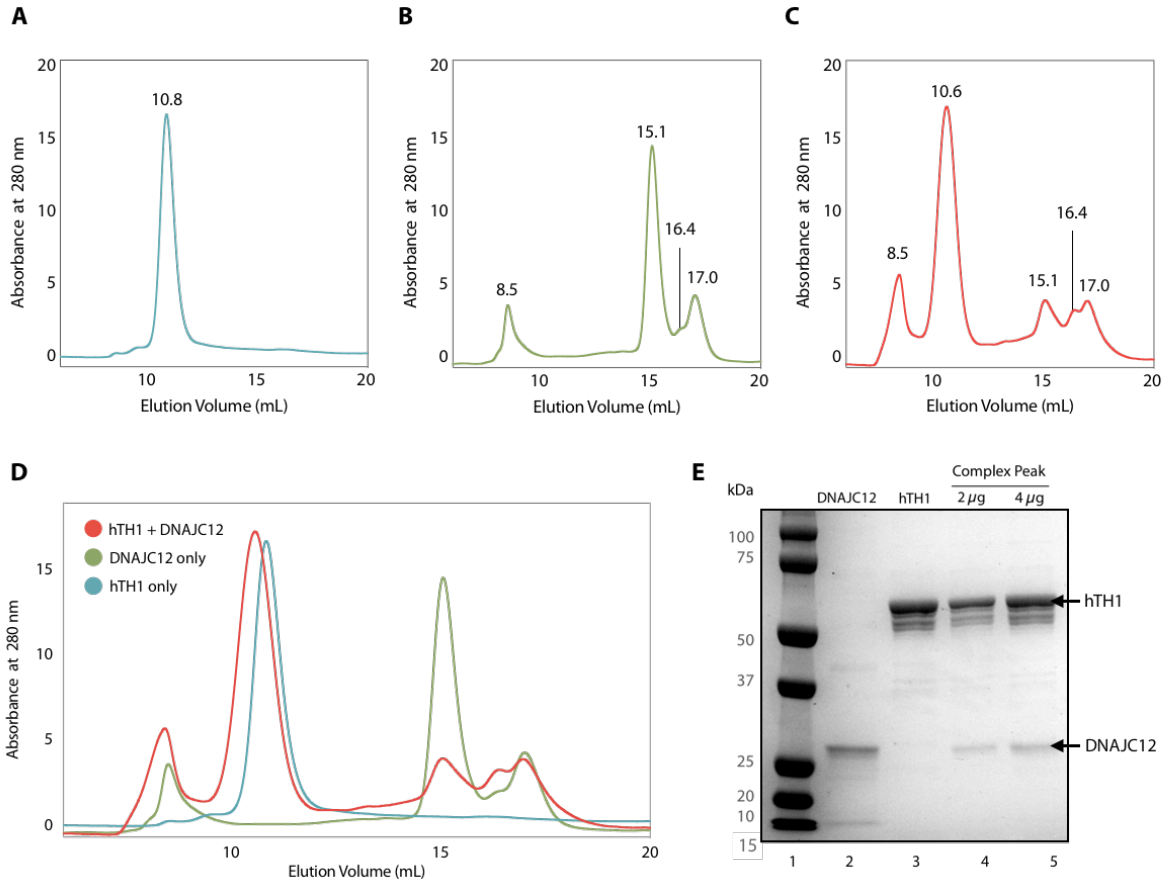

Figure 5-11 Analysis of hTH1 and DNAJC12 Interaction by analytical SEC. Chromatograms obtained using a Superdex™ 200 Increase 10/300 GL column at a flow rate of 0.75 mL/min are shown individually for 100 µg hTH1 only (A), 100 µg purified DNAJC12 only (B) and 100 µg hTH1+ 100 µg purified DNAJC12 (C). Elution volumes in mL are labelled on the individual peaks. (D) Overview of hTH1 and DNAJC12 binding. The three chromatograms are superimposed and presented in red (hTH1+DNAJC12), green (DNAJC12 only) and blue (hTH1 only). (B) Denaturing SDS-PAGE analysis of the predominant peak in the hTH1+DNAJC12 sample. Lane 1: Precision Plus™ Dual Color Standard, lane 2: purified DNAJC12, lane 3: hTH1, lane 4: 2 µg of the complex peak elution, lane 5: 4 µg of complex peak elution.

5.8.2 SEC coupled with Multi-angle Light Scattering (SEC-MALS) Analysis

A SEC-MALS analysis was carried out to determine the molecular weight of the species eluting in the peak corresponding to the complex between DNAJC12 and hTH1. Following the protocol of the initial SEC experiment, the two proteins were incubated together for 10 min at 4 °C prior to analysis. A sample containing only hTH1 was used to determine the increase in size upon complex formation. The molecular weight of hTH1 was determined to be ~232.6 ± 0.1(SD) kDa, corresponding to the size of tetrameric hTH1 calculated from the amino

acid composition (223 kDa), while the complex was ~289.5 ± 0.3(SD) kDa (Figure 5-12). Thus, we observed a clear shift of ~57.2 ± 0.2(SD) kDa in the molecular weights, which strongly indicate hTH1 and DNAJC12 binding.

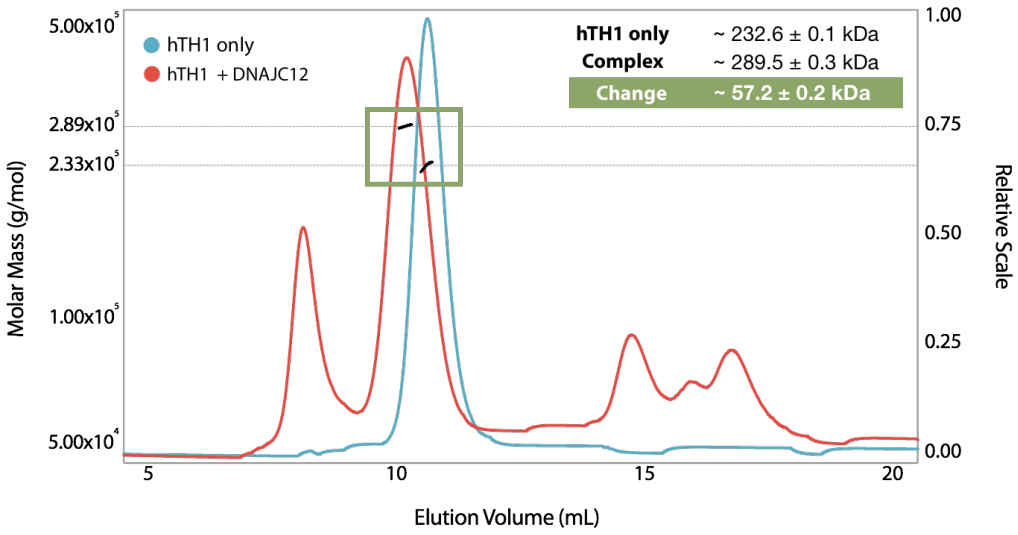

Figure 5-12 SEC-MALS analysis of the hTH1-DNAJC12 complex. The chromatogram shows the absorbance of the hTH1-DNAJC12 complex (red) and hTH1 (blue) samples at 280 nm at their respective elution volumes and the estimated molar mass of each peak (black; green box) as calculated by MALS. SEC-MALS was performed using 100 µg hTH1 only and 100 µg hTH1 + 100 µg purified DNAJC12 on a Superdex™ 200 Increase 10/300 GL column at a flow rate of 0.40 mL/min.

5.8.3 Imaging by EM

In order to visualize and further determine the structure of the complex, samples were prepared for Cryo-EM analysis at Centro Nacional de Biotecnología in Madrid in collaboration with Prof. Valpuesta and Dr. Cuellar. The final results from the analysis were unfortunately not ready in time to be included in this thesis. However, some EM micrographs have been obtained.

5.8.3.1 Preparation of Samples of the hTH1-DNAJC12 Complex

The complex was prepared by scaling up the previous experiments ten-fold and collecting fractions of 250 µL. The whole SEC profile is shown in Figure 5-13A. The fractions that we supposed contained the complex (Fractions 1-8) were analyzed by SDS-PAGE to identify the protein content (Figure 5-13). As expected, all fractions collected from the complex peak contained DNAJC12 (~27 kDa) and hTH1 (~60 kDa).

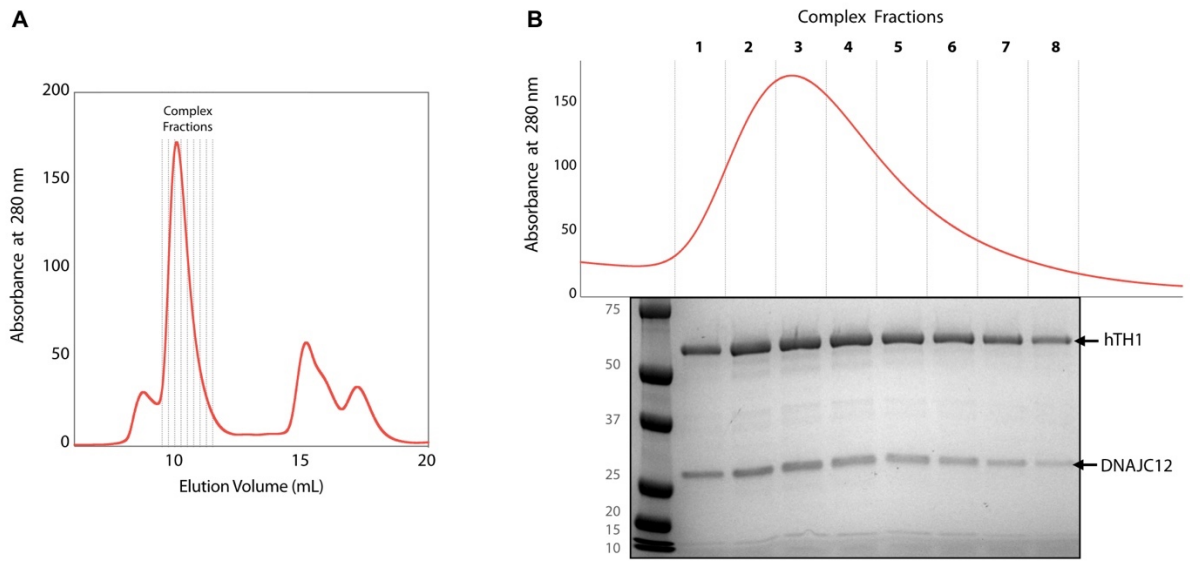

Figure 5-13 Selection of samples of the hTH1-DNAJC12 complex for Cryo-EM. (A) Full chromatogram of the binding sample using a Superdex™ 200 Increase 10/300 GL column at a 0.40 mL/min flow. (B) Partial chromatogram of the binding sample highlighting the 8 collected fractions at elution volume 9-12 mL. Denaturing SDS-PAGE of the eight fractions collected from the complex peak is shown below for the corresponding fraction. The first lane is the Precision Plus™ Dual Color Standard molecular weight ladder.

5.8.3.2 Imaging of the hTH1-DNAJC12 Complex by Electron Microscopy (EM)

The prepared hTH1-DNAJC12 complex sample (Fraction 3; of Figure 5-13B) was first visualized by transmission EM prior to Cryo-EM analysis to ensure sample quality. As seen on Figure 5-14, the complex did not dissociate nor aggregate and was determined by our collaborators in Spain to be homogenous enough for Cryo-EM analysis.

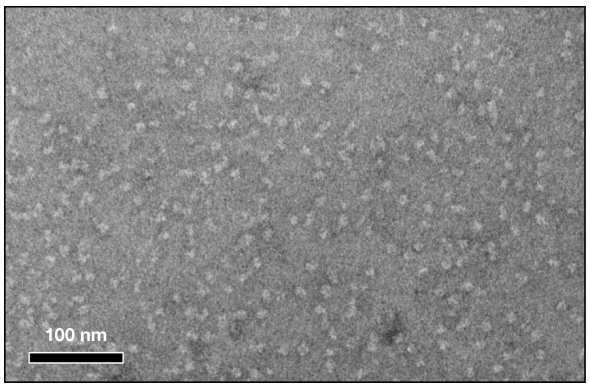

Figure 5-14 hTH1-DNAJC12 complex visualized by electron microscopy. EM image of the hTH1-DNAJC12 complex from Fraction 3 (Figure 5-13B). Scale bar: 100 nm.

5.8.3.3 Analysis of the hTH1-DNAJC12 Complex Formation

Further study of the hTH1-DNAJC12 complex formation was performed by collecting fractions from the SEC chromatogram of the binding sample (Figure 5-13A) in addition to the fractions at the peak representing the complex. These fractions were those eluted at the beginning (early eluting complex; EC) and towards the end of the complex peak (late eluting complex; LC) (Figure 5-15A), and were analyzed by SDS-PAGE (Figure 5-15B) and western blot using antibodies against DNAJC12 (against N-terminus or C-terminus) (Figure 5-15C). Denaturing SDS-PAGE analysis showed that the small void peak contained mostly full-length DNAJC12 (27 kDa) while both DNAJC12 and hTH1 were present in the EC sample (Figure 5-15B).

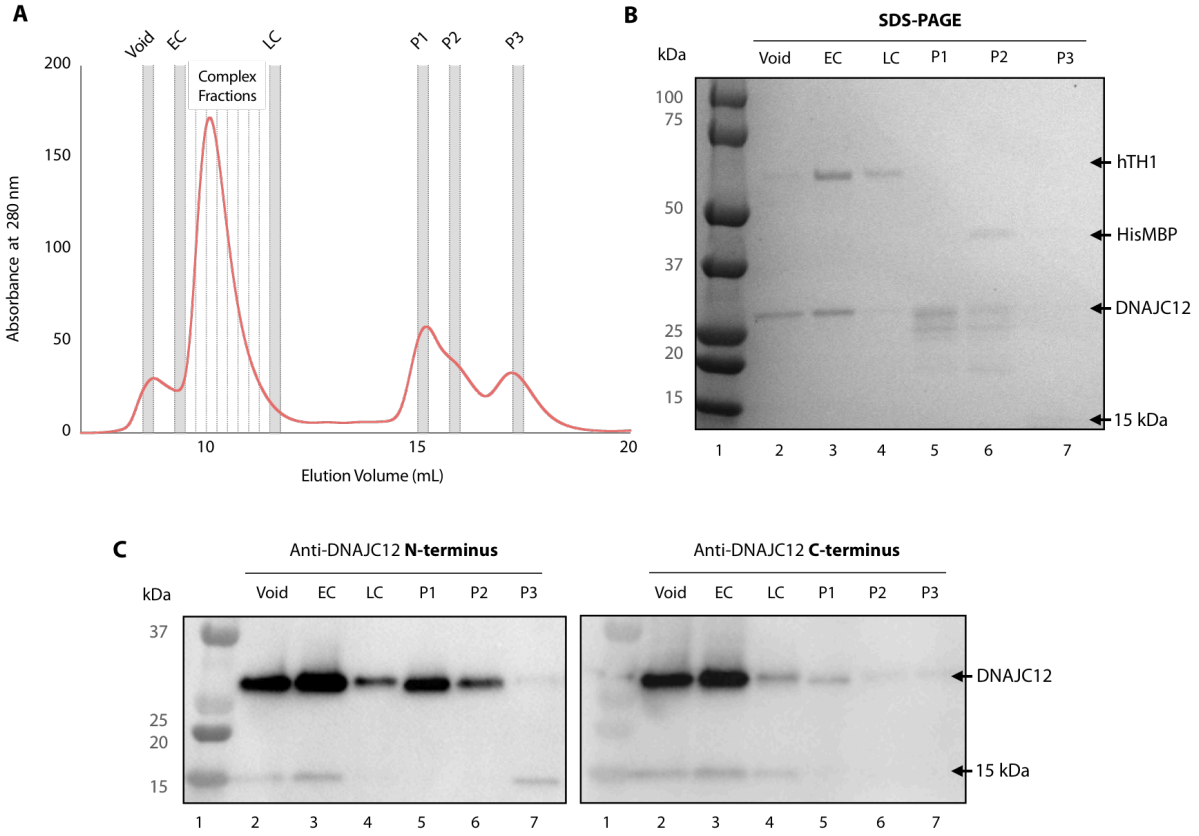

Figure 5-15 Analysis of the hTH1-DNAJC12 complex formation by denaturing SDS-PAGE and immunoblotting. (A) Full chromatogram of the binding sample using a Superdex™ 200 Increase 10/300 GL column at a 0.40 mL/min flow rate highlighting the six collected fractions eluted from the void volume, early eluting complex (EC), the complex fractions (see Figure 5-13), late eluting complex (LC) and the three peaks associated with DNAJC12 (P1, P2 and P3). (B) Denaturing SDS-PAGE analysis of the samples. Lane 1: Precision Plus™ Dual Color Standard; lane 2: void; lane 3: EC; lane 4: LC; lane 5: P1; lane 6: P2; lane 7: P3. (C) Immunoblots of the samples using antibodies against either the N-terminus (left) or C-terminus (right) of DNAJC12.

Although DNAJC12 in the LC was hardly visible by Coomassie stain, immunoblotting confirmed the presence of DNAJC12 (Figure 5-15B;C). The three peaks associated with purified DNAJC12 (P1, P2, P3 in Figure 5-15A) were also found to have different compositions where P1 contained the full length DNAJC12 (27 kDa), while P2 also contained residual HisMBP (43 kDa) from the purification. P3 predominantly contained the ~15 kDa DNAJC12.

Immunoblotting using antibodies against the N- or C-terminus of DNAJC12 both showed detection at ~27 kDa and ~15 kDa in the void and EC samples, suggesting contamination of the EC by species eluting in the void volume (Figure 5-15C). The ~27 kDa band was detected using both antibodies in the LC, P1, P2 and P3 samples. Interestingly, only the N-terminal region of DNAJC12 was detected in the ~15 kDa band in the P3 sample. Conversely, the ~15 kDa band in the LC sample could only be detected using the antibody against the C-terminus but not against the N-terminus.

These results suggest that both N- and C- terminus areas are present in partly digested DNAJC12 (~15 kDa band) in the purified sample (Figure 5-8A), while only the C-terminal region seems to co-elute with the complex. The N-terminal region elutes as P3 or in the void of the complex sample. Although these species present in the ~15 kDa band are not expected to be biologically relevant, they contribute to identify the C-terminal region of DNAJC12 as the area involved in the binding to hTH1.

5.8.4 Analysis of the ~15 kDa DNAJC12 Fragment

To further investigate the possible role of the C-terminal region of DNAJC12 in client binding, the complex and purified DNAJC12 samples were analyzed by SDS-PAGE and the ~15 kDa bands were excised from the gel prior to MS/MS investigation (Figure 5-16A). The final MS/MS results obtained directly from the PROBE facility show that the ~15 kDa protein from the purified DNAJC12 sample yielded 81% coverage of the DNAJC12 sequence, suggesting that both N- and C- terminal parts of degraded DNAJC12 were present (Figure 5-16B).

However, the sample from the hTH1-DNAJC12 complex yielded only 41% coverage of the DNAJC12 sequence, precisely the second half of the protein. These results suggest that

the recombinant DNAJC12 is vulnerable to proteolytic cleavage at a specific site or region, which results in two fragments. Nevertheless, the detection of only the C-terminal region in the ~15 kDa species from the complex sample further supports the notion that the C-terminal region of DNAJC12 is involved in client binding.

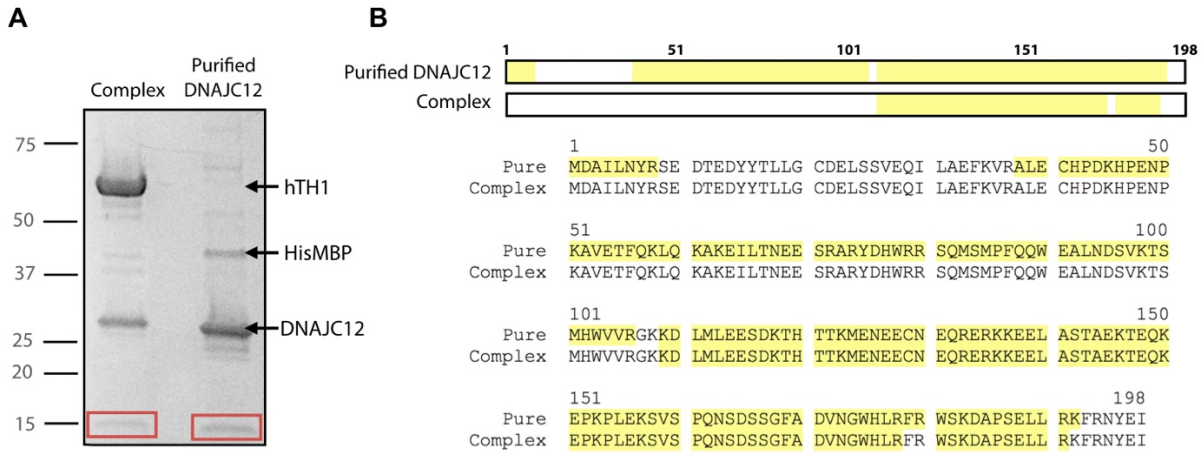

Figure 5-16 Analysis of the ~15 kDa bands from the complex and purified DNAJC12 samples by MS/MS. (A) SDS-PAGE analysis of 5 µg complex and 5 µg purified DNAJC12 sample. The excised bands are highlighted by the red boxes. The Precision Plus™ Dual Color Standard was used as a molecular weight ladder. (B) MS/MS results of the two excised ~15kDa bands (from the complex and purified DNAJC12 samples). Sequences covered by the analysis are highlighted in yellow. Assuming that the full-length DNAJC12 is cleaved at residues 107-108, the theoretical molecular weights of the N- and C-terminal fragments would be approximately 13 and 11 kDa, respectively.

5.8.5 Determination of the Binding Affinity by Surface Plasmon Resonance (SPR)

5.8.5.1 Isolation of the Full-length hTH1-binding DNAJC12

We selected SPR as the method of choice to determine the interaction kinetics and the affinity for the binding of DNAJC12 to hTH1. Despite the very tiny amounts of the C-terminal fragment in the purified DNAJC12 sample, we aimed to eliminate it from the sample prior to the determination of the affinity of binding of DNAJC12 to hTH1 by SPR. We thus performed detailed SEC to isolate the full-length DNAJC12, collecting fractions of 250 µL which were individually analyzed by denaturing SDS-PAGE (Figure 5-17) to check for sample purity. As shown on the gel, the first 3 fractions appeared to contain only DNAJC12 as a single 27 kDa band. The succeeding fractions all contained traces of HisMBP (43 kDa) and/or the ~15 kDa band with degraded DNAJC12, which was the only band observed in the fractions collected towards the end of the peak. Therefore, to ensure the best possible purity, only fractions 1-3 were pooled and used for SPR analysis of the DNAJC12 and hTH1 interaction.

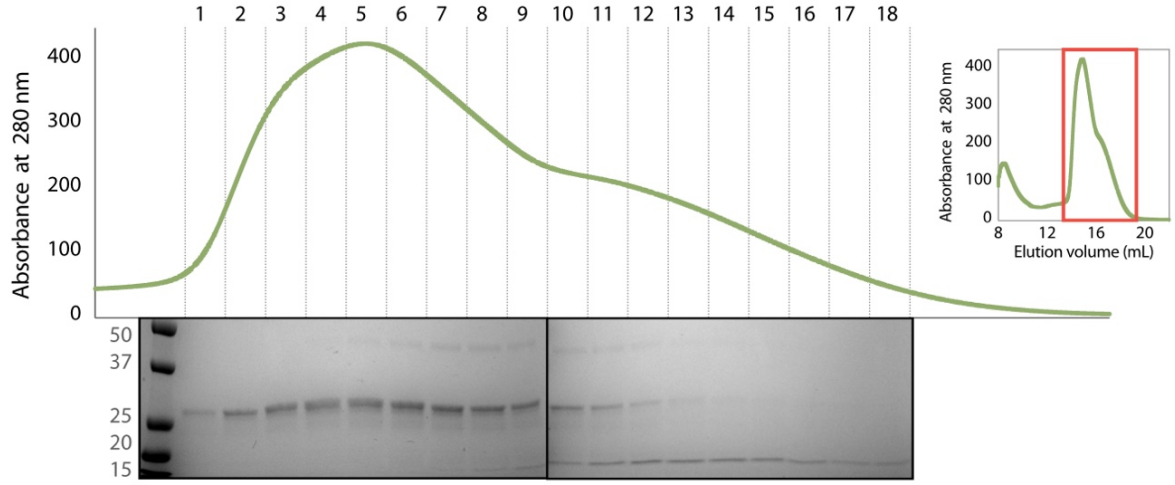

Figure 5-17 Isolation of the full-length hTH1-binding DNAJC12. Partial chromatogram of 7 mg purified DNAJC12 from SEC using a Superdex 200™ 10/300 GL column at 4 °C at a 0.40 mL/min flow rate, highlighting the 18 collected fractions at elution volumes ~14-19 mL. Inset: Purified DNAJC12 chromatogram from elution volumes 8-22 mL. The portion included in the partial chromatogram is highlighted by a red box. Below: Denaturing SDS-PAGE of the 18 collected fractions is shown below for the corresponding fraction. The first lane is the Precision Plus™ Dual Color Standard molecular weight ladder.

5.8.5.2 SPR Measurements

An initial SPR analysis was conducted to verify binding and gain insights into the affinity between DNAJC12 and hTH1. In this experiment, DNAJC12 was injected at different concentrations and allowed to interact with hTH1, which was immobilized on a CM5 chip. As the analyte was injected onto the chip, an increased response was recorded, verifying the interaction between DNAJC12 and hTH1 (Figure 5-18).

On the sensorgrams presented in Figure 5-18A, the steep increase in the relative response recorded upon injection of the analyte showed an immediate binding of DNAJC12 to hTH1. Even after 600 s of washing, the response units (RU) recorded still had not reached the baseline, indicating slow dissociation. The K_D value of the reaction was estimated in two ways – by taking an average value of the K_D calculated based on the obtained association (k_{on}) and dissociation (k_{off}) rate constants from the individual sensorgrams ($K_D = k_{off}/ k_{on}$), which resulted in a value of 303.0 ± 63.7(SE) nM, and by determining the half-maximal binding of DNAJC12 (EC_{50}) by plotting the change in RU as a function versus the varying concentrations of DNAJC12 and fitting to a Langmuir equation (hyperbolic equation), which resulted in an estimated value of 604.9 ± 68.8(SE) nM.

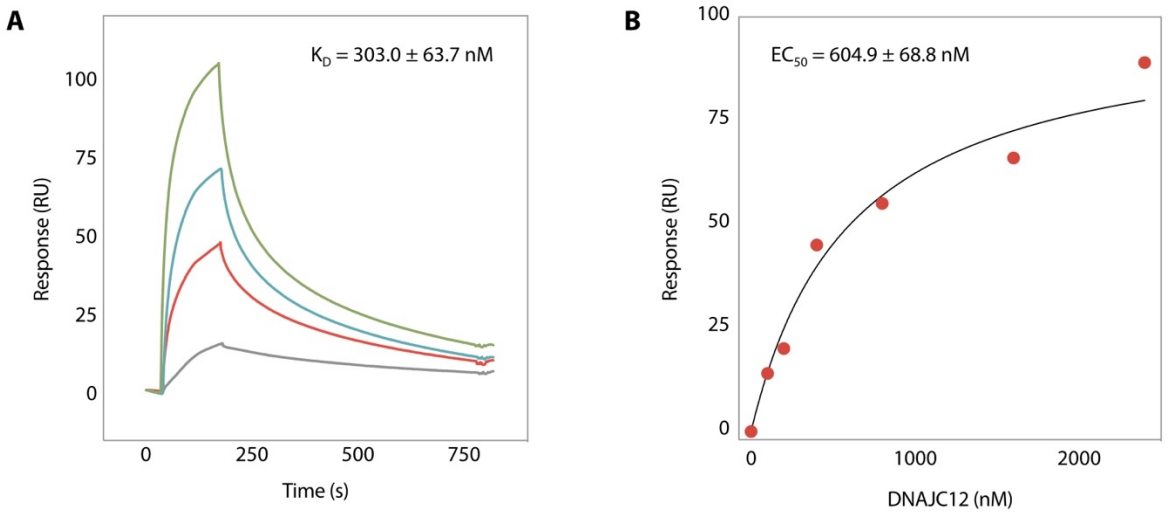

Figure 5-18 SPR analysis of hTH1 and DNAJC12 binding. (A) Sensorgrams of the reaction (using 200 nM (gray), 800 nM (red), 1600 nM (blue), 3200 nM (green) concentrations). The reported K_D is an average of calculated $K_D=k_{off}/k_{on}$ derived from each individual sensorgram. (B) Plot showing the response units recorded versus the concentration of DNAJC12 (0, 100, 200, 400, 800, 1600, 2400 nM) used. The K_D value was obtained by fitting of the data to a hyperbolic binding curve and determining the EC_{50} value.

5.9 Effect of DNAJC12 on the Aggregation of hTH1 Monitored by DLS

The oligomerization of TH beyond the quaternary structure (referred to as aggregation in general) was monitored for 120 min *in vitro* in the presence or absence of DNAJC12 by DLS. The size distribution analyses of the sample by volume and by intensity at 0, 60 or 120 min (Figure 5-19A;B) provided insights on aggregation progression whereas the Z-average value (intensity weighted mean hydrodynamic size of the ensemble) (Figure 5-19C) displayed the time course for increasing particle size in the solution.

It is known that recombinant hTH1 has a tendency to form aggregates over time *in vitro* [49]. The size distribution of hTH1 by volume and by intensity (Figure 5-19A) showed that the isolated TH tetramer has a hydrodynamic diameter of approximately 11.7 nm, as previously determined [88]. The intensity plot indicated that there were some aggregates present in the prepared sample at time 0, but the proportion was so small that they were not observed in the size distribution by volume. At 60 min, the aggregates started appearing in the volume distribution and were seen in the intensity plot as larger in size compared to time 0. Moreover, at 60 min the aggregates were so large that the hTH1 peak at ~11.7 nm, although still comprising 81% of the volume, appeared very small in the intensity plot. By 120 min, almost all the protein had aggregated, as observed in the single peak in both intensity and volume plots.

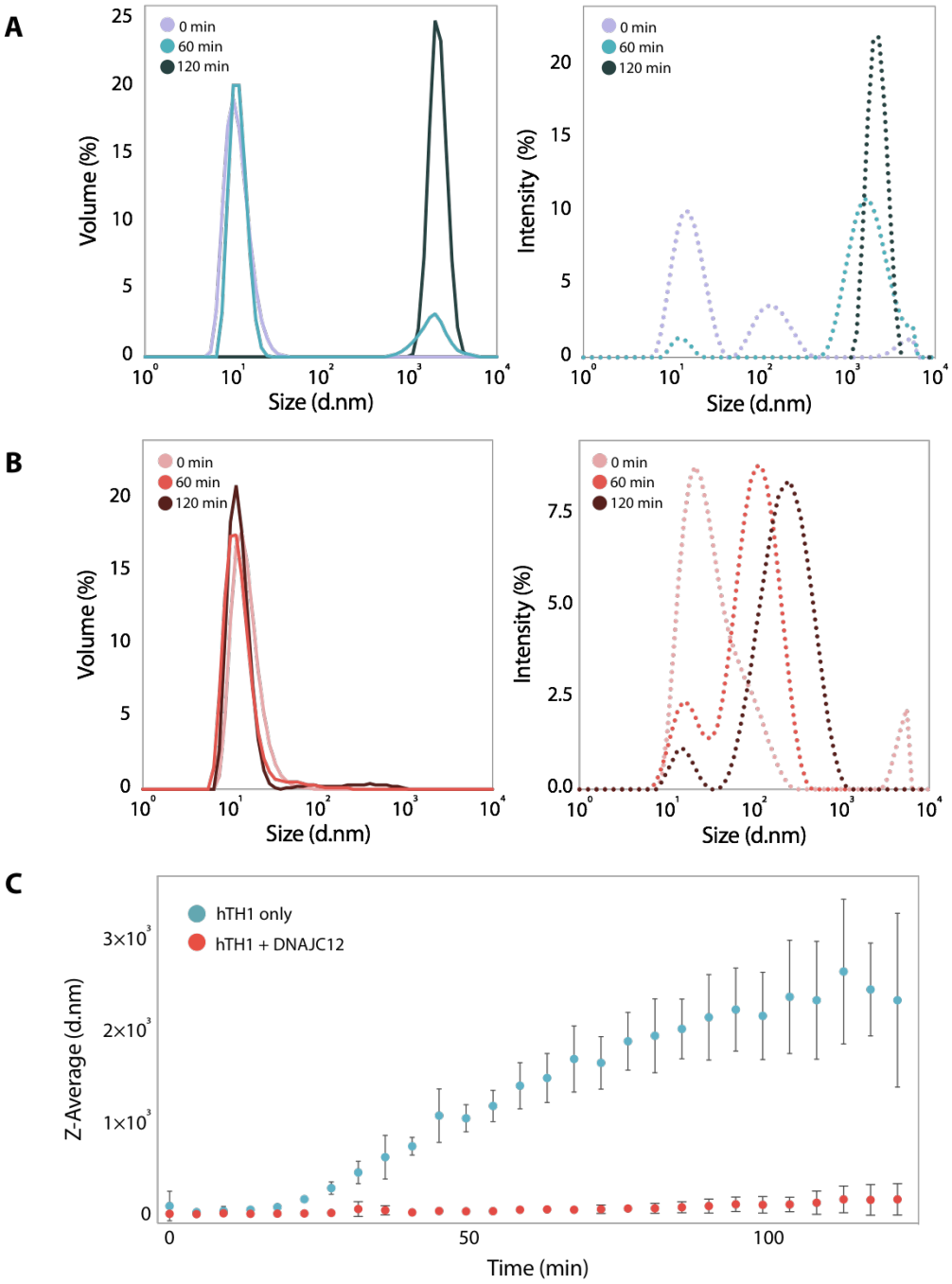

Figure 5-19 Monitoring hTH1 aggregation in the presence or absence of DNAJC12 using DLS. Plots showing the size distribution of the hTH1 sample only (A) and the hTH1 + DNAJC12 sample (B) at 0, 60 and 120 min plotted either by volume or by intensity and comparison of the Z-average values recorded for both hTH1 only (blue) and hTH1 + DNAJC12 (red) samples at 37 °C every 4 min over a 120 min-period from three replicates (C). Error bars indicate standard deviation.

Interestingly, when DNAJC12 was added to hTH1 at the start of the experiment, we observed a large decrease in aggregated forms of hTH1 appearing over time (Figure 5-19B). The size distribution of the sample at 0 min showed the presence of species with a hydrodynamic diameter of approximately 13.5 nm, slightly larger than the control. While the volume plot shows that the sample still mostly comprised of the same species even after

incubating at 37 °C for 60 or 120 min, their respective intensity plots showed that there were aggregates in the sample, but the degree of aggregation was much lower than observed in the hTH1 only sample. The effect of DNAJC12 in delaying hTH1 aggregation is more clearly seen when plotting the time course of the Z-average values recorded over a 120 min period (Figure 5-19C).

6 Discussion

An extensive network of proteins plays a crucial role in the maintenance of protein homeostasis, which when dysregulated may lead to disease [89]. Misfolding diseases such as Parkinson's disease can be caused not only by mutations that lead to misfolding and aggregation, but also by the dysfunction of proteins involved in the proteostasis network [90]. Recently, mutations in the HSP40 co-chaperone protein DNAJC12 have been found to result in phenotypic manifestations of HPA, dystonia and intellectual disabilities with a varying clinical spectrum [38, 64-66, 68] and have been associated with the decreased stability of PAH and TH in human cells [68]. Currently, not much is known about DNAJC12 structure and function, and this Master thesis presents to our knowledge, the first study on the purification and characterization of DNAJC12. This work therefore aims to gain insights into the structure and function of DNAJC12, as well as to study its interaction with one of its clients, TH.

6.1 Full-length DNAJC12 was successfully prepared for functional studies but is vulnerable to proteolysis between the DNAJ domain and C-terminal part

Although genetic studies associating DNAJC12 with PKU and other diseases have increased interest in the protein over the past years [28, 38, 64-66, 68, 71], human DNAJC12 had not been studied *in vitro* prior to this work, due to difficulties in achieving the expression of the protein (Prof. Arturo Muga, University of Basque Country, Spain, personal communication). The strategy employed here was to clone the *DNAJC12* cDNA to produce fusion proteins with three different partners: HisMBP, HisGST and HisZZ. The cloning was successful for pETGST1a/*DNAJC12* and pETMBP1a/*DNAJC12* but only the latter was selected to express the recombinant protein. MBP is one of the most widely used fusion tags due to its ability to increase soluble protein expression by facilitating proper folding of aggregation-prone proteins while also allowing one-step purification of the fusion protein [74, 91]. The expression of HisZZ-DNAJC12 and HisGST-DNAJC12, however, can still be pursued for future work, especially for specific applications such as in the case of GST pull down assays, which would require the production of a GST-tagged fusion protein [92].

Successful initial purification of the 67 kDa HisMBP-DNAJC12 was obtained by expression in LB broth and subsequent purification by amylose affinity chromatography using 20 mM Na-HEPES pH 7.0 buffer with 200 mM NaCl (Figure 5-4). The purification was repeated with buffer supplemented with twice the amount of salt, to possibly increase the electrostatic repulsion between the proteins and improve protein solubility [93], which led to a 2-fold increase in fusion protein yield. Several studies have shown that the use of Terrific Broth instead of Luria-Bertani Broth can further increase protein yield because of its buffering capacity which delays alkalization of the culture [94]. This results in a delayed entry of the culture into the death phase, thus postponing mass cell death which releases proteases that can damage the recombinant protein [95]. As expected, the shift to TB resulted in a further 6.5-fold increase in HisMBP-DNAJC12 yield.

Isolation of DNAJC12 from HisMBP and TEV protease resulted in purified DNAJC12, visualized by SDS-PAGE as a band at 27 kDa, despite the protein being only 24 kDa (Figure 5-5B). Immunoblotting using antibodies against the N- and C- terminal regions of DNAJC12 confirmed the identity of the protein despite the increased apparent molecular weight. An apparent upshift of the expected electrophoretic mobility of DNAJC12 has also been observed in DNAJC12 samples from co-immunoprecipitation [62]. One of the reasons that may explain an altered electrophoretic mobility of purified proteins in SDS-PAGE is an elevated presence of negatively charged residues [96]. Actually, human DNAJC12 presents a patched pattern of basic and acidic residues along its sequence, but it also contains a clearly acidic N-terminal (up to residue 30) (Figure 5-16B).

Surprisingly, a band at ~15 kDa was also detected by immunoblotting using the anti N- and C-terminal DNAJC12 antibodies in the purified sample, indicating that this band is comprised of degraded DNAJC12 species from both the N- and C-terminus (Figure 5-8). This hypothesis was further supported by MS/MS analysis of the excised ~15 kDa band, which detected both N- and C-terminal regions of the protein and sequenced almost the full-length (81% coverage) of the DNAJC12 amino acid sequence in a sample containing proteins that are only ~15 kDa in size (Figure 5-16). Based on this data, recombinant DNAJC12 seems to be particularly susceptible to proteolytic cleavage at a specific site or region, putatively at residues 107-108, dividing the protein in two fragments (~13 kDa N-terminal and ~11 kDa C-terminal fragments) that have an apparent size of ~15 kDa on SDS-PAGE.

6.2 DNAJC12 appears to be a dimer but can also form larger oligomers

SEC analyses of purified protein showed that recombinant DNAJC12 is mainly comprised of apparent dimeric, monomeric and degraded forms in solution (Figure 5-8), but that it can also form larger oligomers (Figure 5-9; Figure 5-10). Measurements based on the calibration of the column measuring the elution of molecular weight markers, pointed to the main population (P1) as a dimer, which is the expected oligomeric organization of DNAJ proteins [19]. Nevertheless, an unequivocal assignment to this population to dimeric DNAJC12 must await the size analysis by a more conclusive method such as SEC-MALS. An initial SEC-MALS analysis of the sample (1 mg/mL) was attempted but did not yield enough light scattering signal to assess the size of the species in the individual peaks as they were too dilute in the sample. The experiment will be later repeated with a higher protein concentration.

Further analysis of the purified DNAJC12 shows that the oligomeric distribution of recombinant DNAJC12 is influenced by the ionic strength of the buffer, as we observe the formation of larger oligomers or aggregates in the absence of salt by DLS (Figure 5-9) and analytical SEC (Figure 5-10). While the structure of the N-terminal region (residues 1-100) has been elucidated by NMR (PDB ID: 2CTQ), nothing is known so far on the structure of the C-terminal region (residues 101-198). *In silico* based prediction programs such as I-TASSER and PrDOS predict the C-terminal region to be mostly disordered (Figure 5-1) and analysis of the sequence shows the presence of high amounts of charged polar amino acid residues (39 out of 98 residues are Arg, Lys, Glu and Asp). This may explain why the absence of salt results in the formation of larger oligomers, as salt in the buffer could provide ions that shield these charged residues, thus keeping them from engaging in intermolecular electrostatic interactions [93].

Although the formation of large oligomers may not be physiologically relevant it is interesting to observe that, while most DNAJ proteins function as dimers, some indeed also function as larger dynamic oligomers. The dimeric co-chaperone DNAJB6 forms dynamic higher order oligomeric forms from dimers which seem to have a role in preventing beta-amyloid aggregation, also keeping the client protein accessible for degradation in an HSP70-independent manner [97]. There is no report about the functional oligomeric form of DNAJC12 in physiologically relevant samples, and our results indicate the relevance of future

investigations of the possible presence of larger oligomers of DNAJC12 under certain conditions in cells and *in vivo* samples.

6.3 DNAJC12 interacts with hTH1 *in vitro*

Initial binding studies in this work using analytical SEC (Figure 5-11), SEC-MALS (Figure 5-12) and SPR (Figure 5-18) confirmed binding of the co-chaperone DNAJC12 to its client hTH1. This data supports previous reports that have identified tyrosine hydroxylase as a client of DNAJC12 [38, 68]. The decrease of the apparent dimer peak as well as the ~57 kDa size increase of the complex compared to the hTH1 control suggests that it is the apparent dimer that binds to hTH1. However, as the size of tetrameric TH was estimated by SEC-MALS to be about 10 kDa higher than expected, it is difficult to conclude about the increase in molecular weight, but the observed size increase is closest to reflect a dimeric form of DNAJC12 (~46 kDa). Thus, awaiting the opportunity to perform more experiments, including the structure determination of the complex, we propose that it is the dimeric form of DNAJC12 that binds to hTH1 under the conditions used.

Upon further investigation, we also detected the ~15 kDa fragment in the complex sample (Figure 5-15B;C), which indicates that the ~15 kDa degraded DNAJC12 binds to hTH1 and that the complex peak may not be as homogenous as previously thought. Unfortunately, due to the suddenly imposed access restrictions to the laboratory, the binding ratio in this experiment was also not optimized and so, it is uncertain whether the DNAJC12 binding capacity of hTH1 was reached. If not, the complex peak is not homogenous, and the size calculated by SEC-MALS would have been an average value [81]. The SEC-MALS analysis of this sample will therefore have to be repeated, using a range of DNAJC12:hTH1 ratios, as well as the isolated full-length DNAJC12 without the ~15 kDa fragment (Figure 5-17). The small amounts obtained of the highly purified sample were sufficient for SPR measurements, but a scale up of the procedure will also allow the use of this sample for detailed SEC-MALS analysis of the complex and other biophysical characterizations.

Binding studies by SPR were used to characterize the interaction between hTH1 and DNAJC12. The co-chaperone bound with high activity, with a K_D-value in the 10^{-1} μM range, in agreement with the steep increase in the recorded response units during the association phase

(large k_{on}) and the slow dissociation phase (small k_{off}) (Figure 5-18). Similar interactions have been found for other chaperone proteins, such as the human DnaJ homolog 2 (HDJ2), which interacts with native progesterone receptor (PR) [98]. The high affinity binding between native PR and HDJ2 suggests that the binding of DNAJ proteins to their client is based more on specific recognition of the client, rather than a more general recognition of misfolded or unfolded regions [98]. The sustained high-affinity interaction between HDJ2 and PR was determined to be crucial for eventual HSP90 chaperoning [98], and in an analogous manner, the same could occur for hTH1, where HSP70 is expected to be recruited by DNAJC12 [62].

6.4 The C-terminal region of DNAJC12 appears to be involved in client binding

The N-terminal region of DNAJC12 contains the J-domain which is common to all J proteins and therefore, it is reasonable to hypothesize that DNAJC12 client specificity is a property of the C-terminal region. In particular, the very C-terminal heptapeptide KFRNYEI is highly conserved in DNAJC12 homologs and has been proposed to be involved in the client recognition [57]. The detection of the DNAJC12 C-terminal region in the ~15 kDa band co-eluting with the complex by western blot (Figure 5-15C) and MS/MS (Figure 5-16) further supports that it is indeed the C-terminal region that is involved in client recognition and binding. We have not yet determined the exact residues involved in the interaction but future experiments with truncated DNAJC12 constructs as well as site-directed mutants are expected to provide more insights into the mechanisms behind the DNAJC12-client interaction.

The predicted disordered structure of the C-terminal region could also be functionally relevant for client recognition as structural flexibility was proposed to be crucial for chaperone function [99]. Structural analysis of the bacterial HSP40 DnaJ in complex with its client RepE further supports this assumption, as EM data suggested that the plasticity of DNAJ dimers allow it to adapt to several substrates [100]. In line with this, disordered chaperones are believed to be conditionally disordered, where unstructured regions adopt specific structures upon binding to their client [101]. This may also be the reason why some *in silico*-based homology modelling and secondary structure prediction show DNAJC12 with several helices (Appendix Figure 10-1) in the C-terminal region but others as almost completely unstructured (Figure 5-1B).

6.5 DNAJC12 delays hTH1 aggregation *in vitro*

The previously described tendency of recombinant hTH1 to form aggregates *in vitro* [49] was utilized in this work to further investigate the effect of the interaction between hTH1 and DNAJC12. Analysis of the size distribution curves by intensity and by volume, as well as Z-average values of hTH1 samples with and without DNAJC12 recorded over a 120-min period indicate that DNAJC12 can prevent hTH1 aggregation in an HSP70-independent manner (Figure 5-19). This phenomenon has been observed in other HSP40s as DNAJB6 and DNAJB8 both directly interact with their client parkin to keep it soluble in a degradation competent state [102]. These chaperones prevent client aggregation by blocking surfaces that could be points of non-productive and aggregating interactions [19]. The SVYFVS (residues 429-434) motif located in the exposed β-strand region of the hTH1 catalytic domain has been previously identified as likely residues involved in amyloid-like aggregation [103]. DNAJC12 could possibly bind to hTH1 in such a way that blocks these residues, thus preventing hTH1 aggregation as observed *in vitro*.

Preliminary experiments using DLS where DNAJC12 is added to hTH1 aggregates also indicate a possible ATP-independent disaggregase function, as observed in the decreasing Z-average values recorded after addition of the chaperone (Appendix Figure 10-2). These preliminary results must however be carefully repeated and confirmed using other techniques because the dissociation of stable aggregates is normally a complex mechanism that usually requires the binding of the HSP40 (DNAJ) protein to the ATP-dependent disaggregase machinery such as the HSP70/HSP110 chaperone system. However, the chaperone protein cpSRP43, which does not have ATPase activity, has been shown to dissociate client aggregates [104].

7 Concluding Remarks

The main objective of this thesis was to gain insights into the structure and function of DNAJC12, as well as the structural determinants and effects of its interaction with hTH1. In this work, we obtained pure recombinant DNAJC12 which allowed us to pursue *in vitro* experiments. We found that recombinant DNAJC12 is mainly comprised of apparent dimeric, monomeric and degraded forms in solution, but may form larger oligomers or aggregates in the absence of salt. In addition, we were able to confirm the interaction between DNAJC12 and hTH1 and have started the isolation of highly pure full-length DNAJC12 samples for more detailed oligomeric and structural studies. It was determined that the apparent dimeric form of DNAJC12 binds to hTH1 with high affinity, and we have gathered evidence that supports the notion that the C-terminal region is involved in client binding. We have also gained insights into the potential role of DNAJC12 in delaying hTH1 aggregation and in dissociating aggregates.

8 Future Perspective

The elucidation of the structure of a protein is fundamental to the understanding of its function. Biophysical techniques such as differential scanning and isothermal titration calorimetries, Cryo-EM and nuclear magnetic resonance, are therefore key techniques for the continuation of this project. Structural data of DNAJC12 on its own and in complex with its client hTH1 are expected to shed light on the chaperone-client interaction and in defining its function, particularly by determining binding stoichiometry and identifying binding interfaces. Preparation of high-quality samples will be crucial to these structural studies, and this work has allowed detecting the vulnerability of recombinant DNAJC12 to proteolysis, as well as pointing to approaches to avoid it. Thus, the transformed cultures could be grown in lower temperatures and also the purification buffers, not only the homogenization buffer, could be supplemented with soluble protease inhibitors, such as Pefabloc®. In any case, we have also shown that it is possible to prepare highly purified samples at low scale (Figure 5-17).

In this study, we have also obtained preliminary evidence that show the potentially diverse functions of DNAJC12, including aggregation prevention and re-solubilization of aggregates. It will also be interesting to investigate these using mutant TH associated with THD, as well as mutant DNAJC12 forms. Recent studies have identified pathogenic variants in *DNAJC12* resulting in a truncated protein product, i.e. p.Trp175Ter [68]. As we hypothesized in this work that the C-terminal is important for client binding, the use of truncated mutants could not only contribute to explain the molecular basis of DNAJC12-client interactions, but also to understand the mechanisms behind the pathogenesis of this mutant.

Furthermore, the ubiquitination of hTH1 when alone and in complex with DNAJC12 by a reconstituted *in vitro* ubiquitination system could not only allow the investigation on the involvement of DNAJC12 in client degradation, as previously demonstrated in studies of PAH in liver extracts [62], but also serve as a tool to map the binding site/s of DNAJC12 to hTH1. Preliminary experiments have already been performed including determining compatible enzymes for ubiquitination (Appendix Figure 10-3) as well as identifying hTH1 ubiquitination sites by tandem mass spectrometry (Appendix Figure 10-4; Figure 10-5), but will have to be continued and repeated in the future.

Lastly, further investigation into the molecular interaction of TH and DNAJC12 should be performed in human cells, including expression of the normal and variant proteins, immunocytochemistry and co-immunoprecipitation, among other techniques. Determining the phenotypic effects of mutant DNAJC12 in cells could provide a better understanding of its function and could also substantiate the studies on aggregation and disaggregation performed *in vitro.*

9 References

1. Hartl, F.U., A. Bracher, and M. Hayer-Hartl, *Molecular chaperones in protein folding and proteostasis.* Nature, 2011. **475**: p. 324-32.
2. Kim, Y.E., M.S. Hipp, A. Bracher, M. Hayer-Hartl, and F.U. Hartl, *Molecular chaperone functions in protein folding and proteostasis.* Annu Rev Biochem, 2013. **82**: p. 323-55.
3. Saluja, A. and D.S. Kalonia, *Nature and consequences of protein-protein interactions in high protein concentration solutions.* Int J Pharm, 2008. **358**: p. 1-15.
4. Dobson, C.M., A. Sali, and M. Karplus, *Protein Folding: A Perspective from Theory and Experiment.* Angew Chem Int Ed Engl, 1998. **37**: p. 868-893.
5. Labbadia, J. and R.I. Morimoto, *The biology of proteostasis in aging and disease.* Annu Rev Biochem, 2015. **84**: p. 435-64.
6. Clausen, L., A.B. Abildgaard, S.K. Gersing, A. Stein, K. Lindorff-Larsen, et al., *Protein stability and degradation in health and disease.* Adv Protein Chem Struct Biol, 2019. **114**: p. 61-83.
7. Hetz, C. and L.H. Glimcher, *Protein homeostasis networks in physiology and disease.* Curr Opin Cell Biol, 2011. **23**: p. 123-5.
8. Hipp, M.S., P. Kasturi, and F.U. Hartl, *The proteostasis network and its decline in ageing.* Nature Reviews Molecular Cell Biology, 2019. **20**: p. 421-435.
9. Thomas, P.J., B.H. Qu, and P.L. Pedersen, *Defective protein folding as a basis of human disease.* Trends Biochem Sci, 1995. **20**: p. 456-9.
10. Willmund, F., M. del Alamo, S. Pechmann, T. Chen, V. Albanèse, et al., *The cotranslational function of ribosome-associated Hsp70 in eukaryotic protein homeostasis.* Cell, 2013. **152**: p. 196-209.
11. Anfinsen, C.B., *Principles that Govern the Folding of Protein Chains.* Science, 1973. **181**: p. 223-230.
12. Jahn, T.R. and S.E. Radford, *The Yin and Yang of protein folding.* FEBS J, 2005. **272**: p. 5962-70.
13. Gregersen, N., P. Bross, S. Vang, and J.H. Christensen, *Protein misfolding and human disease.* Annu Rev Genomics Hum Genet, 2006. **7**: p. 103-24.
14. Zarouchlioti, C., D.A. Parfitt, W. Li, L.M. Gittings, and M.E. Cheetham, *DNAJ Proteins in neurodegeneration: essential and protective factors.* Philos Trans R Soc Lond B Biol Sci, 2018. **373**.
15. Hershko, A. and A. Ciechanover, *The Ubiquitin System.* Annual Review of Biochemistry, 1998. **67**: p. 425-479.
16. Levine, B. and D.J. Klionsky, *Development by Self-Digestion: Molecular Mechanisms and Biological Functions of Autophagy.* Developmental Cell, 2004. **6**: p. 463-477.
17. Saibil, H., *Chaperone machines for protein folding, unfolding and disaggregation.* Nature reviews. Molecular cell biology, 2013. **14**: p. 630-642.
18. Hong, D.S., U. Banerji, B. Tavana, G.C. George, J. Aaron, et al., *Targeting the molecular chaperone heat shock protein 90 (HSP90): lessons learned and future directions.* Cancer Treat Rev, 2013. **39**: p. 375-87.
19. Kampinga, H.H. and E.A. Craig, *The HSP70 chaperone machinery: J proteins as drivers of functional specificity.* Nat Rev Mol Cell Biol, 2010. **11**: p. 579-92.

20. Cheetham, M.E. and A.J. Caplan, *Structure, function and evolution of DnaJ: conservation and adaptation of chaperone function.* Cell Stress Chaperones, 1998. **3**: p. 28-36.
21. Tsai, J. and M.G. Douglas, *A conserved HPD sequence of the J-domain is necessary for YDJ1 stimulation of Hsp70 ATPase activity at a site distinct from substrate binding.* J Biol Chem, 1996. **271**: p. 9347-54.
22. Hageman, J. and H.H. Kampinga, *Computational analysis of the human HSPH/HSPA/DNAJ family and cloning of a human HSPH/HSPA/DNAJ expression library.* Cell Stress Chaperones, 2009. **14**: p. 1-21.
23. Kellner, R., H. Hofmann, A. Barducci, B. Wunderlich, D. Nettels, et al., *Single-molecule spectroscopy reveals chaperone-mediated expansion of substrate protein.* Proc Natl Acad Sci U S A, 2014. **111**: p. 13355-60.
24. Rosenzweig, R., N.B. Nillegoda, M.P. Mayer, and B. Bukau, *The Hsp70 chaperone network.* Nat Rev Mol Cell Biol, 2019. **20**: p. 665-680.
25. Kityk, R., J. Kopp, and M.P. Mayer, *Molecular Mechanism of J-Domain-Triggered ATP Hydrolysis by Hsp70 Chaperones.* Mol Cell, 2018. **69**: p. 227-237 e4.
26. Edvardson, S., Y. Cinnamon, A. Ta-Shma, A. Shaag, Y.-I. Yim, et al., *A deleterious mutation in DNAJC6 encoding the neuronal-specific clathrin-uncoating co-chaperone auxilin, is associated with juvenile parkinsonism.* PloS one, 2012. **7**: p. e36458-e36458.
27. Roosen, D.A., C. Blauwendraat, M.R. Cookson, and P.A. Lewis, *DNAJC proteins and pathways to parkinsonism.* FEBS J, 2019. **286**: p. 3080-3094.
28. Tummala, H., A.J. Walne, M. Williams, N. Bockett, L. Collopy, et al., *DNAJC21 Mutations Link a Cancer-Prone Bone Marrow Failure Syndrome to Corruption in 60S Ribosome Subunit Maturation.* Am J Hum Genet, 2016. **99**: p. 115-24.
29. Valastyan, J.S. and S. Lindquist, *Mechanisms of protein-folding diseases at a glance.* Disease Models & Mechanisms, 2014. **7**: p. 9.
30. Pey, A.L., F. Stricher, L. Serrano, and A. Martinez, *Predicted effects of missense mutations on native-state stability account for phenotypic outcome in phenylketonuria, a paradigm of misfolding diseases.* American journal of human genetics, 2007. **81**: p. 1006-1024.
31. Cheng, S.H., R.J. Gregory, J. Marshall, S. Paul, D.W. Souza, et al., *Defective intracellular transport and processing of CFTR is the molecular basis of most cystic fibrosis.* Cell, 1990. **63**: p. 827-834.
32. Irvine, G.B., O.M. El-Agnaf, G.M. Shankar, and D.M. Walsh, *Protein aggregation in the brain: the molecular basis for Alzheimer's and Parkinson's diseases.* Molecular medicine (Cambridge, Mass.), 2008. **14**: p. 451-464.
33. Haataja, L., T. Gurlo, C.J. Huang, and P.C. Butler, *Islet Amyloid in Type 2 Diabetes, and the Toxic Oligomer Hypothesis.* Endocrine Reviews, 2008. **29**: p. 303-316.
34. Scriver, C.R., R.C. Eisensmith, S.L.C. Woo, and S. Kaufman, *The Hyperphenylalaninemias of Man and Mouse.* Annual Review of Genetics, 1994. **28**: p. 141-166.
35. Gersting, S.W., K.F. Kemter, M. Staudigl, D.D. Messing, M.K. Danecka, et al., *Loss of function in phenylketonuria is caused by impaired molecular motions and conformational instability.* American journal of human genetics, 2008. **83**: p. 5-17.
36. Scriver, C.R., *The PAH gene, phenylketonuria, and a paradigm shift.* Human Mutation, 2007. **28**: p. 831-845.
37. Thony, B. and N. Blau, *Mutations in the GTP cyclohydrolase I and 6-pyruvoyl-tetrahydropterin synthase genes.* Hum Mutat, 1997. **10**: p. 11-20.

38. Anikster, Y., T.B. Haack, T. Vilboux, B. Pode-Shakked, B. Thony, et al., *Biallelic Mutations in DNAJC12 Cause Hyperphenylalaninemia, Dystonia, and Intellectual Disability.* Am J Hum Genet, 2017. **100**: p. 257-266.
39. Huttlin, E.L., L. Ting, R.J. Bruckner, F. Gebreab, M.P. Gygi, et al., *The BioPlex Network: A Systematic Exploration of the Human Interactome.* Cell, 2015. **162**: p. 425-440.
40. Korner, G., D. Noain, M. Ying, M. Hole, M.I. Flydal, et al., *Brain catecholamine depletion and motor impairment in a Th knock-in mouse with type B tyrosine hydroxylase deficiency.* Brain, 2015. **138**: p. 2948-2963.
41. Flydal, M.I. and A. Martinez, *Phenylalanine hydroxylase: function, structure, and regulation.* IUBMB Life, 2013. **65**: p. 341-9.
42. Fitzpatrick, P.F., *The aromatic amino acid hydroxylases.* Adv Enzymol Relat Areas Mol Biol, 2000. **74**: p. 235-94.
43. Li, D. and L. He, *Meta-analysis shows association between the tryptophan hydroxylase (TPH) gene and schizophrenia.* Hum Genet, 2006. **120**: p. 22-30.
44. Mossner, R., K.R. Muller-Vahl, N. Doring, and M. Stuhrmann, *Role of the novel tryptophan hydroxylase-2 gene in Tourette syndrome.* Mol Psychiatry, 2007. **12**: p. 617-9.
45. Fossbakk, A., R. Kleppe, P.M. Knappskog, A. Martinez, and J. Haavik, *Functional studies of tyrosine hydroxylase missense variants reveal distinct patterns of molecular defects in Dopa-responsive dystonia.* Human mutation, 2014. **35**: p. 880-890.
46. Levitt, M., S. Spector, A. Sjoerdsma, and S. Udenfriend, *Elucidation of the Rate-Limiting Step in Norepinephrine Biosynthesis in the Perfused Guinea-Pig Heart.* J Pharmacol Exp Ther, 1965. **148**: p. 1-8.
47. Kaneda, N., K. Kobayashi, H. Ichinose, F. Kishi, A. Nakazawa, et al., *Isolation of a novel cDNA clone for human tyrosine hydroxylase: alternative RNA splicing produces four kinds of mRNA from a single gene.* Biochem Biophys Res Commun, 1987. **146**: p. 971-5.
48. Skjærven, L., K. Teigen, and A. Martinez, *Structure–Function Relationships in the Aromatic Amino Acid Hydroxylases Enzyme Family: Evolutionary Insights.* eLS, 2014.
49. Bezem, M.T., A. Baumann, L. Skjaerven, R. Meyer, P. Kursula, et al., *Stable preparations of tyrosine hydroxylase provide the solution structure of the full-length enzyme.* Sci Rep, 2016. **6**: p. 30390.
50. Waløen, K., R. Kleppe, A. Martinez, and J. Haavik, *Tyrosine and tryptophan hydroxylases as therapeutic targets in human disease.* Expert Opinion on Therapeutic Targets, 2017. **21**: p. 167-180.
51. Andersson, K.K., C. Vassort, B.A. Brennan, L. Que, Jr., J. Haavik, et al., *Purification and characterization of the blue-green rat phaeochromocytoma (PC12) tyrosine hydroxylase with a dopamine-Fe(III) complex. Reversal of the endogenous feedback inhibition by phosphorylation of serine-40.* Biochem J, 1992. **284 (Pt 3)**: p. 687-95.
52. Kansy, J.W., S.C. Daubner, A. Nishi, N. Sotogaku, M.D. Lloyd, et al., *Identification of tyrosine hydroxylase as a physiological substrate for Cdk5.* Journal of neurochemistry, 2004. **91**: p. 374-384.
53. Ghorbani, S., P.D. Szigetvari, J. Haavik, and R. Kleppe, *Serine 19 phosphorylation and 14-3-3 binding regulate phosphorylation and dephosphorylation of tyrosine hydroxylase on serine 31 and serine 40.* Journal of Neurochemistry, 2020. **152**: p. 29-47.

54. Almas, B., B. Le Bourdelles, T. Flatmark, J. Mallet, and J. Haavik, *Regulation of recombinant human tyrosine hydroxylase isozymes by catecholamine binding and phosphorylation.* European Journal of Biochemistry, 1992. **209**: p. 249-255.
55. Itagaki, C., T. Isobe, M. Taoka, T. Natsume, N. Nomura, et al., *Stimulus-coupled interaction of tyrosine hydroxylase with 14-3-3 proteins.* Biochemistry, 1999. **38**: p. 15673-80.
56. Jorge-Finnigan, A., R. Kleppe, K. Jung-Kc, M. Ying, M. Marie, et al., *Phosphorylation at serine 31 targets tyrosine hydroxylase to vesicles for transport along microtubules.* J Biol Chem, 2017. **292**: p. 14092-14107.
57. Lee, J., Y. Hahn, J.H. Yun, K. Mita, and J.H. Chung, *Characterization of JDP genes, an evolutionarily conserved J domain-only protein family, from human and moths.* Biochimica et Biophysica Acta (BBA) - Gene Structure and Expression, 2000. **1491**: p. 355-363.
58. Choi, J., S. Djebbar, A. Fournier, and C. Labrie, *The co-chaperone DNAJC12 binds to Hsc70 and is upregulated by endoplasmic reticulum stress.* Cell Stress Chaperones, 2014. **19**: p. 439-46.
59. Cunningham, F., P. Achuthan, W. Akanni, J. Allen, M.R. Amode, et al., *Ensembl 2019.* Nucleic Acids Res, 2019. **47**: p. D745-D751.
60. Fagerberg, L., B.M. Hallstrom, P. Oksvold, C. Kampf, D. Djureinovic, et al., *Analysis of the human tissue-specific expression by genome-wide integration of transcriptomics and antibody-based proteomics.* Mol Cell Proteomics, 2014. **13**: p. 397-406.
61. Consortium, G.T., *The Genotype-Tissue Expression (GTEx) project.* Nat Genet, 2013. **45**: p. 580-5.
62. Jung-Kc, K., N. Himmelreich, K.S. Prestegard, T.S. Shi, T. Scherer, et al., *Phenylalanine hydroxylase variants interact with the co-chaperone DNAJC12.* Hum Mutat, 2019. **40**: p. 483-494.
63. de Sain-van der Velden, M.G.M., W.F.E. Kuper, M.A. Kuijper, L.A.T. van Kats, H. Prinsen, et al., *Beneficial Effect of BH4 Treatment in a 15-Year-Old Boy with Biallelic Mutations in DNAJC12.* JIMD Rep, 2018. **42**: p. 99-103.
64. Veenma, D., D. Cordeiro, N. Sondheimer, and S. Mercimek-Andrews, *DNAJC12-associated developmental delay, movement disorder, and mild hyperphenylalaninemia identified by whole-exome sequencing re-analysis.* Eur J Hum Genet, 2018. **26**: p. 1867-1870.
65. Straniero, L., I. Guella, R. Cilia, L. Parkkinen, V. Rimoldi, et al., *DNAJC12 and dopa-responsive nonprogressive parkinsonism.* Ann Neurol, 2017. **82**: p. 640-646.
66. van Spronsen, F.J., N. Himmelreich, V. Rufenacht, N. Shen, D.V. Vliet, et al., *Heterogeneous clinical spectrum of DNAJC12-deficient hyperphenylalaninemia: from attention deficit to severe dystonia and intellectual disability.* J Med Genet, 2017. **55**: p. 249-253.
67. Feng, Y., S. Liu, C. Tang, X. Jiang, F. Tang, et al., *Identification of an inherited pathogenic DNAJC12 variant in a patient with hyperphenylalalinemia.* Clin Chim Acta, 2019. **490**: p. 172-175.
68. Gallego, D., F. Leal, A. Gámez, M. Castro, R. Navarrete, et al., *Pathogenic variants of DNAJC12 and evaluation of the encoded cochaperone as a genetic modifier of hyperphenylalaninemia.* Human Mutation, 2020. **In press**.
69. de Alcantara Filho, P.R., F.R. Mangone, A.C. Pavanelli, S.A. de Bessa Garcia, S. Nonogaki, et al., *Gene expression profiling of triple-negative breast tumors with*

different expression of secreted protein acidic and cysteine rich (SPARC). Breast Cancer Management, 2018. **7**: p. BMT09.
70. He, H.L., Y.E. Lee, H.P. Chen, C.H. Hsing, I.W. Chang, et al., *Overexpression of DNAJC12 predicts poor response to neoadjuvant concurrent chemoradiotherapy in patients with rectal cancer.* Exp Mol Pathol, 2015. **98**: p. 338-45.
71. Uno, Y., M. Kanda, T. Miwa, S. Umeda, H. Tanaka, et al., *Increased Expression of DNAJC12 is Associated with Aggressive Phenotype of Gastric Cancer.* Ann Surg Oncol, 2019. **26**: p. 836-844.
72. Bogomolovas, J., B. Simon, M. Sattler, and G. Stier, *Screening of fusion partners for high yield expression and purification of bioactive viscotoxins.* Protein Expr Purif, 2009. **64**: p. 16-23.
73. Svasti, J. and B. Panijpan, *SDS-polyacrylamide gel electrophoresis. A simple explanation of why it works.* Journal of Chemical Education, 1977. **54**: p. 560.
74. Duong-Ly, K.C. and S.B. Gabelli, *Affinity Purification of a Recombinant Protein Expressed as a Fusion with the Maltose-Binding Protein (MBP) Tag.* Methods Enzymol, 2015. **559**: p. 17-26.
75. Pattenden, L.K. and W.G. Thomas, *Amylose affinity chromatography of maltose-binding protein: purification by both native and novel matrix-assisted dialysis refolding methods.* Methods Mol Biol, 2008. **421**: p. 169-89.
76. Bornhorst, J.A. and J.J. Falke, *Purification of proteins using polyhistidine affinity tags.* Methods Enzymol, 2000. **326**: p. 245-54.
77. Chaga, G., M. Widersten, L. Andersson, J. Porath, U.H. Danielson, et al., *Engineering of a metal coordinating site into human glutathione transferase M1-1 based on immobilized metal ion affinity chromatography of homologous rat enzymes.* Protein Eng, 1994. **7**: p. 1115-9.
78. Hagel, L. and J.-C. Janson, *Chapter 6 Size-exclusion chromatography*, in *Journal of Chromatography Library*, E. Heftmann, Editor. 1992, Elsevier. p. A267-A307.
79. Yau, W.W. and D.D. Bly, *Effect of Solute Shape or Conformation in Size Exclusion Chromatography*, in *Size Exclusion Chromatography (GPC)*. 1980, American Chemical Society. p. 197-206.
80. Stetefeld, J., S.A. McKenna, and T.R. Patel, *Dynamic light scattering: a practical guide and applications in biomedical sciences.* Biophysical reviews, 2016. **8**: p. 409-427.
81. Some, D., H. Amartely, A. Tsadok, and M. Lebendiker, *Characterization of Proteins by Size-Exclusion Chromatography Coupled to Multi-Angle Light Scattering (SEC-MALS).* JoVE, 2019: p. e59615.
82. Homola, J., S.S. Yee, and G. Gauglitz, *Surface plasmon resonance sensors: review.* Sensors and Actuators B: Chemical, 1999. **54**: p. 3-15.
83. Drescher, D.G., D. Selvakumar, and M.J. Drescher, *Analysis of Protein Interactions by Surface Plasmon Resonance.* Adv Protein Chem Struct Biol, 2018. **110**: p. 1-30.
84. Yang, J., R. Yan, A. Roy, D. Xu, J. Poisson, et al., *The I-TASSER Suite: protein structure and function prediction.* Nat Methods, 2015. **12**: p. 7-8.
85. Ishida, T. and K. Kinoshita, *PrDOS: prediction of disordered protein regions from amino acid sequence.* Nucleic acids research, 2007. **35**: p. W460-W464.
86. Pace, C.N., F. Vajdos, L. Fee, G. Grimsley, and T. Gray, *How to measure and predict the molar absorption coefficient of a protein.* Protein Sci, 1995. **4**: p. 2411-23.
87. van den Berg, S., P.A. Lofdahl, T. Hard, and H. Berglund, *Improved solubility of TEV protease by directed evolution.* J Biotechnol, 2006. **121**: p. 291-8.

88. Kleppe, R., S. Rosati, A. Jorge-Finnigan, S. Alvira, S. Ghorbani, et al., *Phosphorylation dependence and stoichiometry of the complex formed by tyrosine hydroxylase and 14-3-3gamma.* Mol Cell Proteomics, 2014. **13**: p. 2017-30.
89. Sinnige, T., A. Yu, and R.I. Morimoto, *Challenging Proteostasis: Role of the Chaperone Network to Control Aggregation-Prone Proteins in Human Disease.* Adv Exp Med Biol, 2020. **1243**: p. 53-68.
90. Klaips, C.L., G.G. Jayaraj, and F.U. Hartl, *Pathways of cellular proteostasis in aging and disease.* J Cell Biol, 2018. **217**: p. 51-63.
91. Esposito, D. and D.K. Chatterjee, *Enhancement of soluble protein expression through the use of fusion tags.* Curr Opin Biotechnol, 2006. **17**: p. 353-8.
92. *Detection of protein-protein interactions using the GST fusion protein pull-down technique.* Nature Methods, 2004. **1**: p. 275-276.
93. Tsumoto, K., D. Ejima, A.M. Senczuk, Y. Kita, and T. Arakawa, *Effects of salts on protein-surface interactions: applications for column chromatography.* J Pharm Sci, 2007. **96**: p. 1677-90.
94. Kram, K.E. and S.E. Finkel, *Rich Medium Composition Affects Escherichia coli Survival, Glycation, and Mutation Frequency during Long-Term Batch Culture.* Applied and environmental microbiology, 2015. **81**: p. 4442-4450.
95. Kour, D., K.L. Rana, S. Thakur, S. Sharma, N. Yadav, et al., *Chapter 3 - Disruption of Protease Genes in Microbes for Production of Heterologous Proteins*, in *New and Future Developments in Microbial Biotechnology and Bioengineering*, H.B. Singh, V.K. Gupta, and S. Jogaiah, Editors. 2019, Elsevier: Amsterdam. p. 35-75.
96. Matagne, A., B. Joris, and J.M. Frere, *Anomalous behaviour of a protein during SDS/PAGE corrected by chemical modification of carboxylic groups.* Biochem J, 1991. **280 (Pt 2)**: p. 553-6.
97. Hageman, J., M.A. Rujano, M.A.W.H. van Waarde, V. Kakkar, R.P. Dirks, et al., *A DNAJB Chaperone Subfamily with HDAC-Dependent Activities Suppresses Toxic Protein Aggregation.* Molecular Cell, 2010. **37**: p. 355-369.
98. Hernández, M.P., A. Chadli, and D.O. Toft, *HSP40 binding is the first step in the HSP90 chaperoning pathway for the progesterone receptor.* The Journal of biological chemistry, 2002. **277**: p. 11873-11881.
99. Weikl, T., K. Abelmann, and J. Buchner, *An unstructured C-terminal region of the hsp90 co-chaperone p23 is important for its chaperone function11Edited by R. Huber.* Journal of Molecular Biology, 1999. **293**: p. 685-691.
100. Cuellar, J., J. Perales-Calvo, A. Muga, J.M. Valpuesta, and F. Moro, *Structural insights into the chaperone activity of the 40-kDa heat shock protein DnaJ: binding and remodeling of a native substrate.* J Biol Chem, 2013. **288**: p. 15065-74.
101. Bardwell, J.C. and U. Jakob, *Conditional disorder in chaperone action.* Trends Biochem Sci, 2012. **37**: p. 517-25.
102. Kakkar, V., E.F.E. Kuiper, A. Pandey, I. Braakman, and H.H. Kampinga, *Versatile members of the DNAJ family show Hsp70 dependent anti-aggregation activity on RING1 mutant parkin C289G.* Scientific Reports, 2016. **6**: p. 34830.
103. Baumann, A., A. Jorge-Finnigan, K. Jung-Kc, A. Sauter, I. Horvath, et al., *Tyrosine Hydroxylase Binding to Phospholipid Membranes Prompts Its Amyloid Aggregation and Compromises Bilayer Integrity.* Scientific reports, 2016. **6**: p. 39488-39488.
104. Jaru-Ampornpan, P., K. Shen, V.Q. Lam, M. Ali, S. Doniach, et al., *ATP-independent reversal of a membrane protein aggregate by a chloroplast SRP subunit.* Nature structural & molecular biology, 2010. **17**: p. 696-702.

10 Appendix

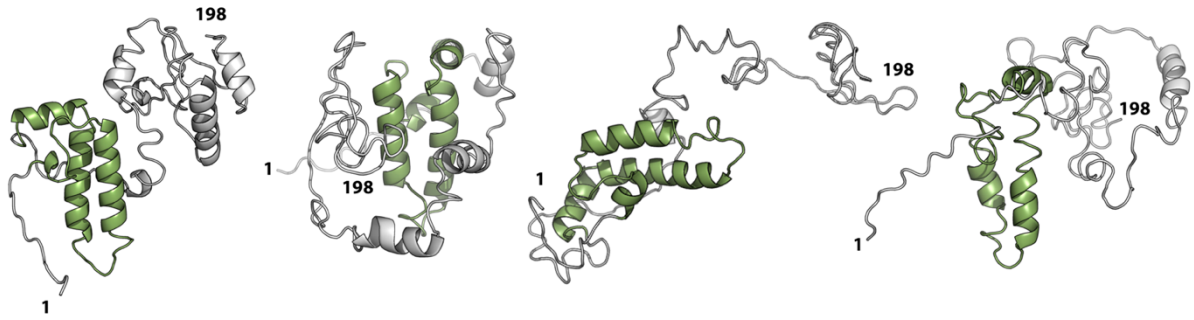

Figure 10-1 DNAJC12 structures predicted by I-TASSER. The J-domain (residues 14-79) is highlighted in green.

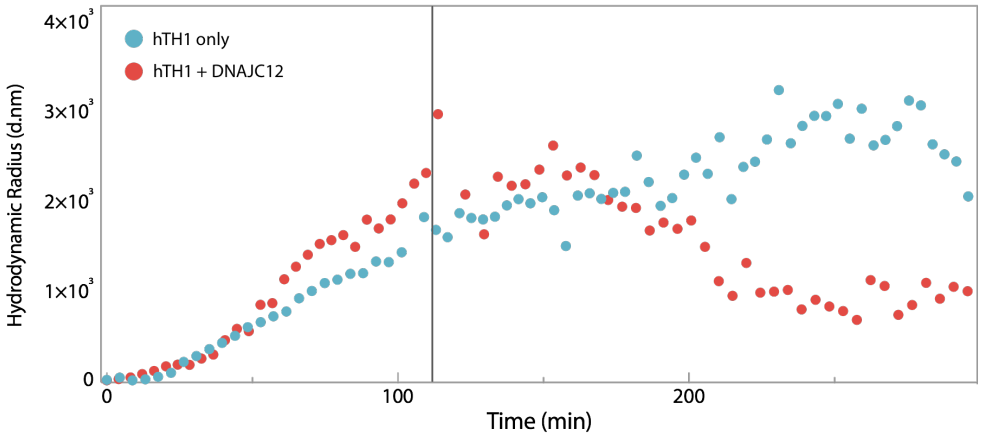

Figure 10-2 Monitoring potential disaggregation after addition of DNAJC12 to hTH1 aggregates by DLS. Comparison of the Z-average values recorded for both hTH1 only (blue) and hTH1 + DNAJC12 (red) samples every 4 min over a 300 min-period. DNAJC12 or buffer was added at the 110-min mark, as denoted by the black line.

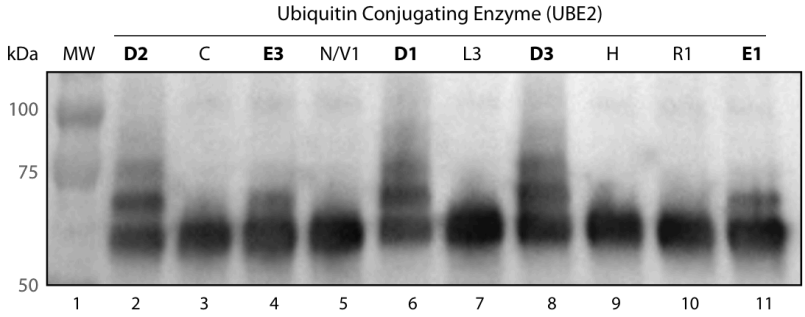

Figure 10-3 Optimization of the ubiquitination of hTH1 using a reconstituted *in vitro* ubiquitination system. Western blot analysis of hTH1 *in vitro* ubiquitination reactions using antibodies against TH. The *in vitro* ubiquitination assay was optimized using 10 different recombinant Human UbcH E2 enzymes that best suited the E3 enzyme CHIP to generate ubiquitinated hTH1 species. Since ubiquitin is ~8 kDa, we expect that addition of ubiquitin subunits would increase the molecular weight of hTH1 by 8 kDa. Western blot analysis using antibodies against hTH1 show that reactions containing the D1, D2 and D3 E2 enzymes yielded three bands with estimated sizes of 60 kDa, 68 kDa and 77 kDa. This corresponds very well with the non-ubiquitinated (56 kDa, ~60 kDa band), monoubiquitinated and polyubiquitinated forms of hTH1. Reactions containing E3 and E1 enzymes showed only two bands corresponding with non-ubiquitinated and monoubiquitinated hTH1, while all other tested E2 enzymes did not show hTH1 ubiquitination. Lane 1 contains the Precision Plus™ Dual Color Standard molecular weight ladder, while lanes 2-11 contain ubiquitination samples using different UBE2 enzymes (as indicated above).

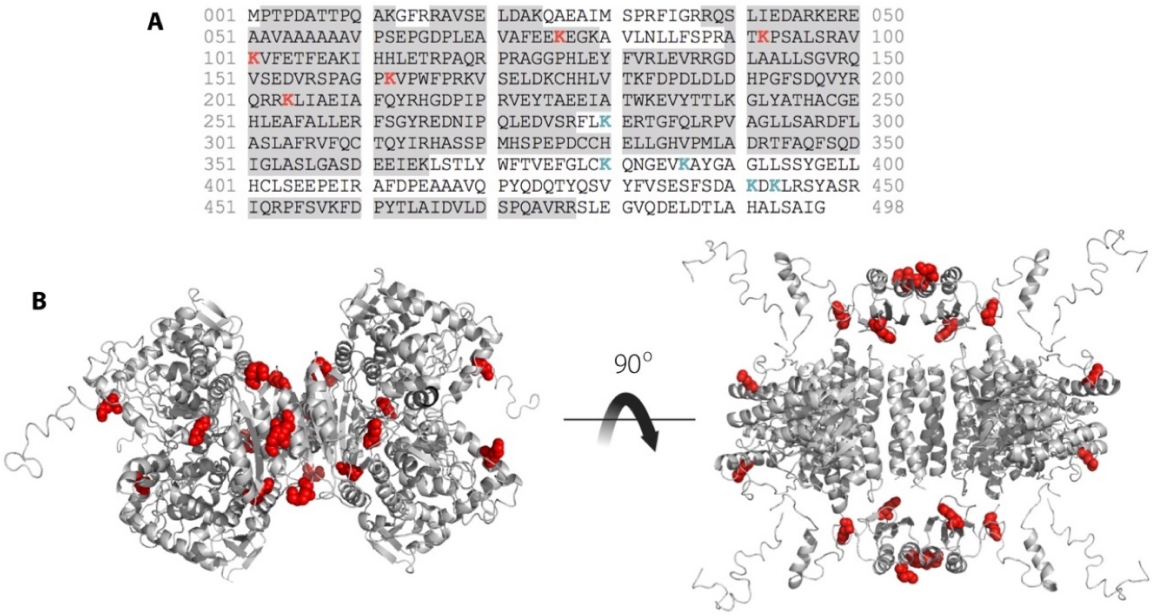

Figure 10-4 Identified ubiquitination sites on hTH1 by MS/MS. With the standard conditions used for *in vitro* ubiquitination (60 min incubation; 37 °C), five lysine residues (highlighted in red – K76, K92, K101, K162 and K204) were either GG- or LRGG- modified and identified as ubiquitination sites in the 379 out of 498 amino acids covered by the MS/MS results (highlighted in gray). Other lysine residues not covered by MS/MS analysis are highlighted in blue (A). The five lysine residues identified as ubiquitination sites were labelled in the full length SAXS structure of hTH1 (SASBD ID: SASDBZ4) as red spheres [48] (B).

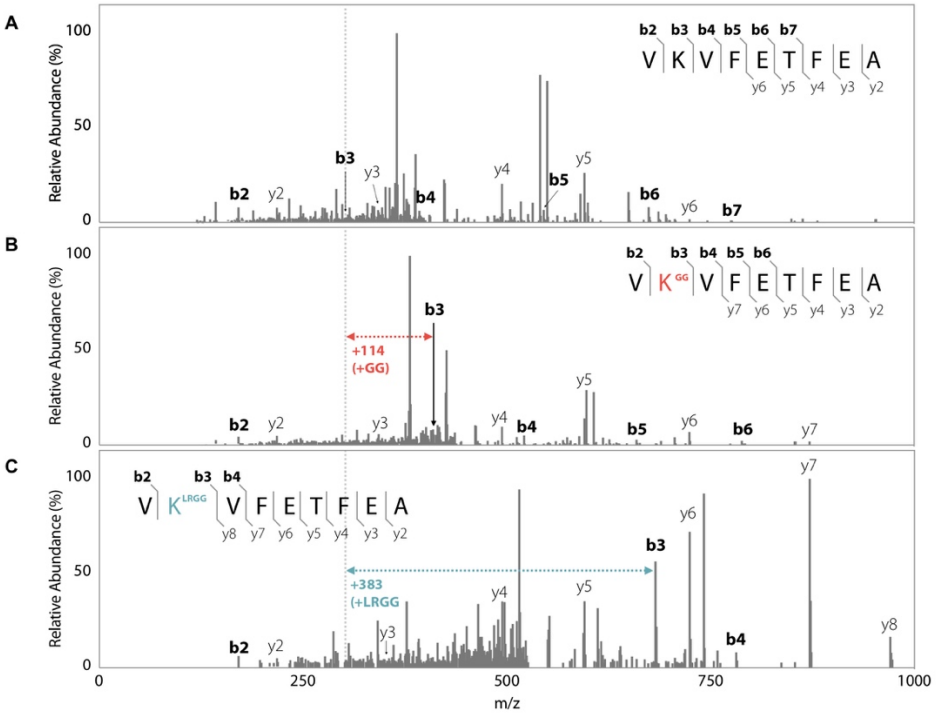

Figure 10-5 Sample MS/MS results showing modified and unmodified K101. Ubiquitinated lysine residues were identified on the hTH1 sequence by the addition of the ubiquitin C-terminal dipeptide GG or tetrapeptide LRGG, which are known ubiquitin remnant peptides. The addition of these peptides results in a mass shift of 114 or 383 Da for +GG (B) or +LRGG (C) modifications, respectively, as compared to the unmodified (A) K101 residue on the sample spectra of the oligopeptide VKVFETFEA (hTH1 residues 100-108).